GEOSPHERE

GEOSPHERE

https://doi.org/10.1130/GES02466.1

17 figures; 1 set of supplemental files

CORRESPONDENCE: jeffapplebenowitz@gmail.com

CITATION: Benowitz, J.A., Roeske, S.M., Regan, S.P., Waldien, T.S., Elliott, J.L., and O'Sullivan, P.B., 2022, Large-scale, crustal-block vertical extrusion between the Hines Creek and Denali faults coeval with slip localization on the Denali fault since ca. 45 Ma. Haves Range, Alaska, USA: Geosphere. https://doi.org/10.1130/GES02466.1

Science Editor: Andrea Hampel Associate Editor: Christopher J. Spencer

Received 1 July 2021 Revision received 24 November 2021 Accepted 31 December 2021

Published online 7 April 2022





This paper is published under the terms of the CC-BY-NC license

© 2022 The Authors

Large-scale, crustal-block vertical extrusion between the Hines **Creek and Denali faults coeval with slip localization on the Denali** fault since ca. 45 Ma, Hayes Range, Alaska, USA

Jeff A. Benowitz¹, Sarah M. Roeske², Sean P. Regan³, Trevor S. Waldien⁴, Julie L. Elliott⁵, and Paul B. OʻSullivan⁶

²Earth and Planetary Sciences, University of California, Davis, California 95616, USA

³Geophysical Institute, University of Alaska Fairbanks, Fairbanks, Alaska 99775, USA

⁴Department of Geology and Geological Engineering, South Dakota School of Mines and Technology, South Dakota 57701, USA

Department of Earth and Environmental Sciences, Michigan State University, Michigan 48824, USA

⁶GeoSep Services, Moscow, Idaho 83843, USA

ABSTRACT

Oblique convergence along strike-slip faults can lead to both distributed and localized deformation. How focused transpressive deformation is both localized and maintained along sub-vertical wrench structures to create high topography and deep exhumation warrants further investigation. The high peak region of the Hayes Range, central Alaska, USA, is bound by two lithospheric scale vertical faults: the Denali fault to the south and Hines Creek fault to the north. The high topography area has peaks over 4000 m and locally has experienced more than 14 km of Neogene exhumation, yet the mountain range is located on the convex side of the Denali fault Mount Hayes restraining bend, where slip partitioning alone cannot account for this zone of extreme exhumation. Through the application of U-Pb zircon, 40Ar/39Ar (hornblende, muscovite, biotite, and K-feldspar), apatite fission-track, and (U-Th)/He geo-thermochronology, we test whether these two parallel, reactivated suture zone structures are working in tandem to vertically extrude the Between the Hines Creek and Denali faults block on the convex side of the Mount Hayes restraining bend. We document that since at least 45 Ma, the Denali fault has been bent and localized in a narrow fault zone (<160 m) with a significant dip-slip component, the Mount Hayes restraining bend has been fixed to the north side of the Denali fault, and that the Between the Hines Creek and Denali faults block has been undergoing vertical extrusion as a relatively coherent block along the displacement "free faces" of two lithospheric scale suture zone faults. A bent Denali fault by ca. 45 Ma supports the long-standing Alaska orocline hypothesis that has Alaska bent by ca. 44 Ma. Southern Alaska is currently converging at ~4 mm/yr to the north against the Denali fault and driving vertical extrusion of the Between the Hines Creek and Denali faults block and deformation north of the Hines Creek fault. We apply insights ascertained from the Between the Hines Creek and Denali faults block to another region in southern Alaska, the Fairweather Range, where

extreme topography and persistent exhumation is also located between two sub-parallel faults, and propose that this region has likely undergone vertical extrusion along the free faces of those faults.

INTRODUCTION

Deformation and associated topography along strike-slip faults is commonly correlated with oblique convergence (Spotila et al., 2007). Known boundary conditions along strike-slip fault systems that localize transpressive deformation are variations in fault dip (Fattaruso et al., 2014), rheology (Niemi et al., 2013), and/or geometric complexities (Roeske et al., 2007; Mann, 2007). This localization of deformation along strike-slip faults is often accommodated by flower structures in the upper crust (e.g., Sylvester, 1988). Nevertheless, extreme topographic elements adjacent to the master strand of a strike-slip fault system also exist (e.g., Liquiñe-Ofqui fault: Lara et al., 2008; Fairweather fault: McAleer et al., 2009; southern San Andreas fault: Moser et al., 2017; Alpine fault: Klepeis et al., 2019) with no obvious link to geometric features, rheology, or dip-slip splay faults. In these examples, the presence of paired, sub-vertical structures may play a role in these high, vertical tectonic environs.

Reactivated suture zones can involve two or more parallel structures following ocean basin closure (Dewey, 1977; Gansser, 1980; Sone and Metcalfe, 2008; Mueller et al., 2019). Parallel structures can also develop when forearc slivers and continental fragments are accreted or translated into place (Garver and Davidson, 2015; Alvarado et al., 2016; Schartman et al., 2019). Reactivated suture zone bounding structures typically are sub-vertical (Brennan et al., 2011), offset the Moho (Fichtner et al., 2013), are regions of weakness (Bailey et al., 2000), and are not linked at depth (Sippl, 2016; Westerweel et al., 2020). Therefore, reactivated suture bounding faults and paired sub-vertical faults in general have the potential to act as zones of weakness, which we refer to as free-faces, which facilitate displacement and allow large-scale, crustal-block vertical extrusion in response to regional stress fields.

Jeff Benowitz https://orcid.org/0000-0003-2294-9172

In this study we integrate new thermochronological investigations with existing thermochronological data sets to evaluate whether the characteristics of two sub-parallel, reactivated suture zone faults are responsible in part for the creation of the asymmetrical Alaska Range. The Alaska Range is the topographic expression of the dextral Denali fault system (e.g., Jadamec et al., 2013), which in Alaska occurs within the Mesozoic suture zone between the Wrangellia composite terrane and terranes of North American affinity (Fig. 1)

(e.g., Trop et al., 2020). To the west of Broad Pass in the central Alaska Range, the highest topography of North America lies on the concave side (south) of the Mount McKinley migrating restraining bend (see Burkett et al., 2016), but to the east of Broad Pass in the Hayes Range, the highest topography lies inexplicably on the convex side (north) of the Denali fault's gentle 13° Mount Hayes restraining bend (Fig.1). The high peak region of the Hayes Range, including Mount Hayes (4216 m), is located between the Hines Creek and Denali faults,

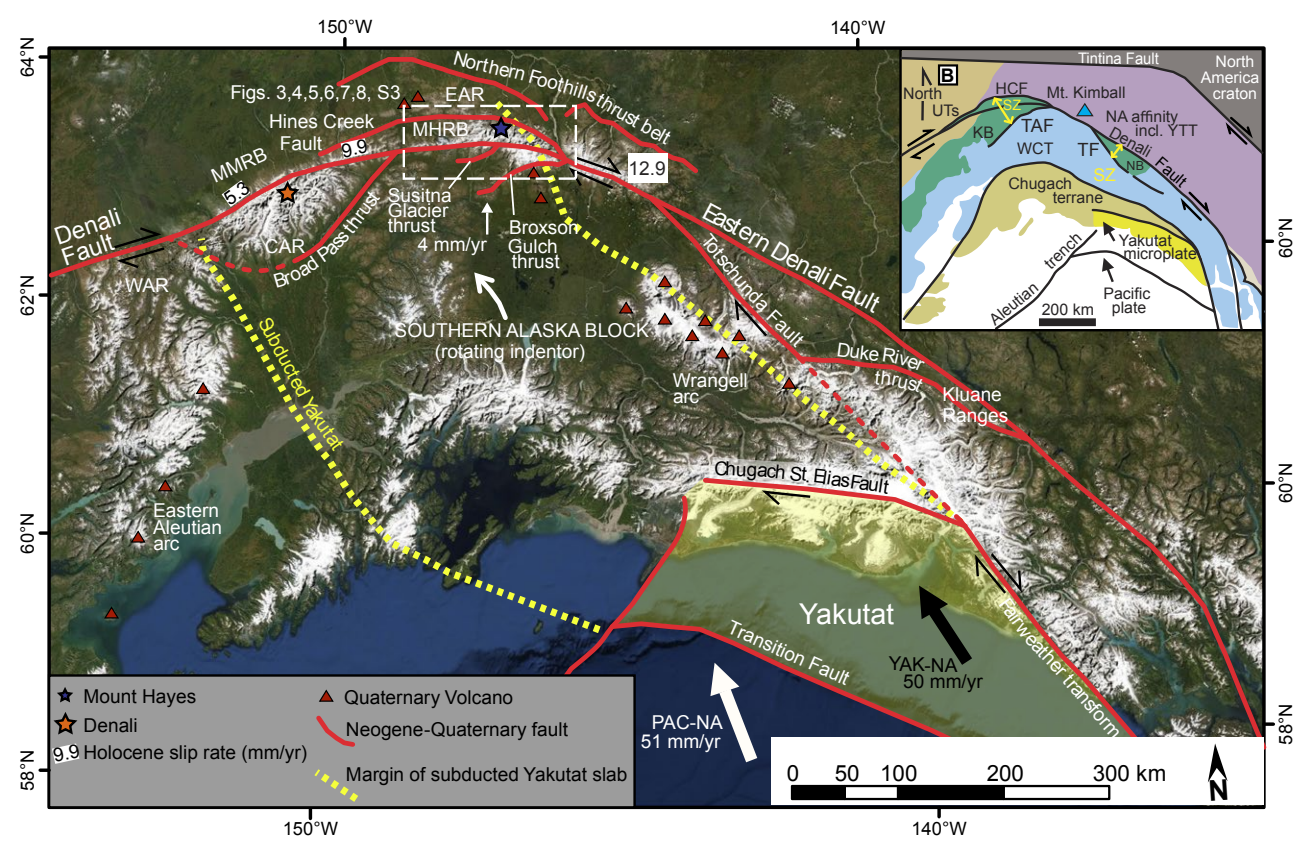


Figure 1. (A) Digital Globe satellite image of south-central Alaska shows the locations of Neogene–Quaternary fault systems discussed in the text, subducted and un-subducted portions of the Yakutat microplate (yellow), Quaternary volcanoes (red triangles), and the locations of Figures 3-8 and S3 (see text footnote 1; dashed white box). Denali fault Holocene slip rates are from Haeussler et al. (2017). Pacific–North America (PAC-NA) and Yakutat microplate–North America (YAK-NA) vectors are from Elliott et al. (2010). Margin of subducted Yakutat microplate is based chiefly on tomography and seismicity data (adapted from Eberhart-Phillips et al., 2006; Bauer et al., 2014; and Wech, 2016). Convergence rate-vector (4.1 mm/yr) for southern Alaska in reference to the apex of the Mount Hayes restraining bend apex calculated for this study is based on the geodetic model of Elliott and Freymueller (2020). WAR—Western Alaska Range, CAR—Central Alaska Range, EAR—Eastern Alaska Range, MMRB—Mount McKinley restraining bend, MHRB—Mount Hayes restraining bend. (B) Inset in upper right shows the simplified terrane geology in the region of the satellite image including the Cretaceous suture zone separating Wrangellia composite terranes, NA—North America, YTT—Tukon-Tanana terrane, WCT—Wrangellia composite terrane.

which indicates possible involvement of these paired Alaska Range structures in large-scale, crustal block vertical extrusion. This region records over 14 km of Neogene exhumation along the Denali fault (Benowitz et al., 2011a, 2014, 2019) (Figs. 1–2). Furthermore, we assess another region of focused exhumation and extreme topography along the Fairweather Transform for similar large-scale block uplift between aligned lithospheric-scale, sub-vertical faults.

Alaska Range Suture Zone

The Mesozoic to Cenozoic Alaska Range suture zone is the borderland between the peri-Laurentian Yukon-Tanana composite terrane (North American continental margin and Yukon-Tanana terrane) to the north and accreted, late Paleozoic and Mesozoic intra-oceanic arc rocks of the accreted Wrangellia composite terrane to the south (Fig. 1; Jones et al., 1982; Nokleberg et al., 1985; Trop and Ridgway, 2007; Dusel-Bacon et al., 2013; Jones et al., 2017). Rocks within the Alaska Range suture zone consist primarily of the Kahiltna and Nutzotin basins (Fig. 1B), which are composed principally of Late Jurassic to Late Cretaceous marine sedimentary strata and metamorphic equivalents (Ridgway et al., 2002; Trop et al., 2020). The extent of Neogene vs. early Cenozoic shortening (e.g., Trop et al., 2019) and the composition of the current basement to these strata is a subject of debate (Romero et al., 2020; Keough and Ridgway, 2021). More recent work has led to the conclusion that labeling all of the continentally derived rocks to the north as North American affinity and considering the Kahiltna as one basin oversimplifies regions with complex geologic histories (Hults et al., 2013; Dusel-Bacon et al., 2017; Dumoulin et al., 2018, Box et al., 2019, Waldien et al., 2021a). In this paper, these vestigial terms are used for simplicity and because the true geologic complexity inherited from the Mesozoic holds no sway on the scope of this work.

The Denali fault locally marks the lithospheric boundary between continental margin assemblages to the north and the Wrangellia composite terrane to the south, in the regions where no marine basin is preserved, between the Totschunda and Hines Creek faults' intersections with the Denali fault (Fig. 1B). In contrast, our study focuses on the region of maximum width of the suture zone, where geophysical data sets indicate that the Alaska Range suture zone is delineated by the crustal-scale Hines Creek fault to the north and the Talkeetna fault to the south (Fig. 1B; Brennan et al., 2011; Miller et al., 2018), although Mesozoic-Cenozoic deformation extends beyond the region between these major faults (Ridgway et al., 2002; Bemis et al., 2015). The metamorphosed North American crust is ~26-30 km thick north of the Hines Creek fault, whereas the Wrangellia composite terrane crust has been imaged to be ~30-48 km thick south of the Denali fault and possibly increases in thickness from west to east (Veenstra et al., 2006; Fuis et al., 2008; Brennan et al., 2011; Allam et al., 2017; Miller et al., 2018). Between the continental margin and the Wrangellia composite terrane is the dissected and imbricate Mesozoic Kahiltna marine basin with a generally undetermined basement (Romero et al., 2020; Keough and Ridgway, 2021), resulting in a total crustal thickness of ~41 km thick, as shown by P receiver functions (Miller et al., 2018).

In the Mount Kimball region of the eastern Alaska Range, rheological contrasts may explain why the highest topography is north of the Denali fault. Along that segment of the fault, relatively thin crust dominated by quartz-rich rocks is juxtaposed directly against the thick, mafic crust of the Wrangellia composite terrane (Fig. 1B) (Fitzgerald et al., 2014, 2018). In our region of study, the Denali fault dissects the remnant Mesozoic marine basin of the Alaska Range suture zone (Trop et al., 2019); thus, no obvious crustal-scale rheologic contrast exists across the Denali fault to explain the location of focused exhumation on the convex side of the Mount Hayes restraining bend (e.g., Romero et al., 2020).

Denali Fault

The 2000-km-long, dextral strike-slip Denali fault traverses the Alaska Range suture zone and has been active since at least ca. 65 Ma (Miller et al., 2002;

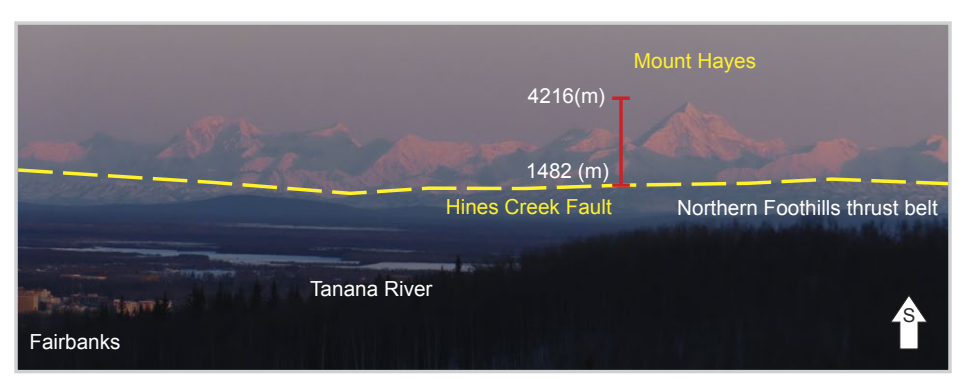


Figure 2. Photo of the Hayes Range was taken looking south from Fairbanks, Alaska. The Hines Creek fault is the topographic break between the Northern Foothills thrust belt (Fig. 1A), the Tanana River Valley, and the high mountains of the Hayes Range, which rise dramatically starting south of the Hines Creek fault. Photo was taken from the lead author's porch (64.9061N°, 147.7912W°; World Geodetic System 1984).

Benowitz et al., 2014; Waldien et al., 2021a). The modern trace of the Denali fault is arcuate, with an azimuth that varies by over 50° (Fig. 1). Regan et al. (2021) investigated two similarly aged plutons as piercing points to establish that the Denali fault has been curved since ca. 33 Ma with horizontal slip rates decreasing east to west from ~9 mm/yr to ~4 mm yr averaged over the long-term, which is similar in ratio to Pleistocene–Holocene rates of ~12 mm/yr to ~5 mm/yr (Haeussler et al., 2017). Slip has been taken up on contractional structures on both sides of the Denali fault since at least the Oligocene (Riccio et al., 2014; Bemis et al., 2015; Burkett et al., 2016; Waldien et al., 2021b), which supports evidence of a long-lived oblique slip, strike-slip fault system (Fig. 1). Additionally, the current northwestward motion of southern Alaska relative to interior Alaska results in ~4 mm/yr of convergence with the central Denali fault (Fig. 1) (Bemis et al., 2015; Elliott and Freymueller, 2020). How the rocks between the Hines Creek and Denali faults respond to this impingement and why the most extreme exhumation is localized in this area is the focus of this study.

Although some geophysical studies do not show significant offset of the Moho across the Denali fault in the Alaska Range suture zone (Veenstra et al., 2006; Brennan et al., 2011), several other studies indicate that the fault likely penetrates the entire lithosphere. A more recent geophysical study images it as a sub-vertical structure that penetrates the lithosphere and offsets the Moho by 10–15 km (Allam et al., 2017). Additionally, the Denali fault has likely been tapping mantle sources of magma since at least 40 Ma, based on the occurrence of late Eocene plutons with arc chemistry distributed along and truncated by

the active fault (Fig. 3) (Regan et al., 2020, 2021). A 3-D geodynamic model of deformation across southern Alaska requires a lithospheric scale weak zone to generate significant topography along the fault and to match the neotectonic block motions of southern Alaska (Jadamec et al., 2013).

Hines Creek Fault

The ~300-km-long Hines Creek fault system was assumed to be inactive based on the inference that the mapped trace was intruded by a ca. 95 Ma pluton (Wahrhaftig et al., 1975). More recent work has demonstrated that various strands of the Hines Creek fault system have been active throughout the Cenozoic and remain active today. Thermochronological analysis (this study), the presence of an Oligocene basin between two strands of the Hines Creek fault system (Nokleberg et al., 1992), paleoseismological studies (Federschmidt, 2014), historic seismicity, and detailed mapping (Nokleberg et al., 2013) document Cenozoic activity on the main fault strand and active splays near the fault's intersection with the Denali fault. The Hines Creek fault system also manifests as the topographic break between the high peak region of the Hayes Range and the Northern Foothills thrust belt (Bemis and Wallace, 2007; Bemis et al., 2012) and Tanana basin to the north (Fig. 2).

Though the Hines Creek fault has been imaged as a lithospheric-scale structure offsetting the Moho (Veenstra et al., 2006; Brennan et al., 2011; Allam

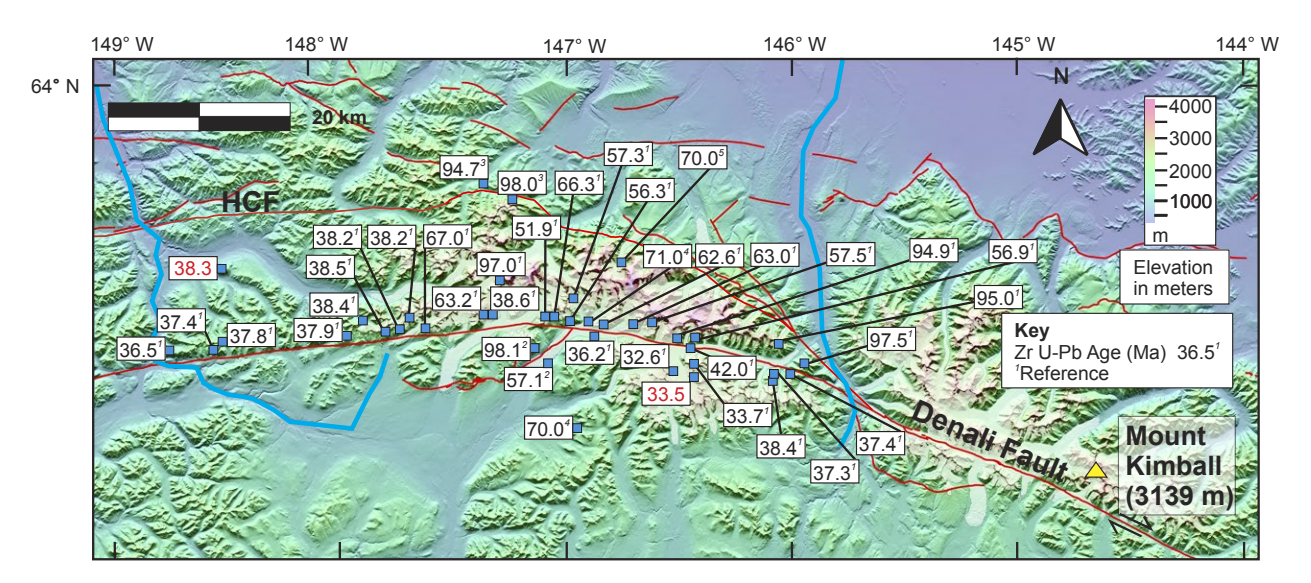


Figure 3. Digital elevation model depicts the high peak region of the eastern Alaska Range (U.S. Geological Survey Shuttle Radar Topography Mission, 30 m) with sample locations and U-Pb zircon crystallization ages (in Ma) from new (red) and published (black) samples for plutons north and south of the Denali fault. HCF—Hines Creek fault. Sample references: ¹Regan et al. (2021); ²Riccio et al. (2014); ³Nokleberg et al. (2013); ⁴Nokleberg et al. (1992); ⁵Aleinikoff et al. (1987).

et al., 2017), the fault's role in the formation of the Alaska Range has not received much, if any, attention. The amount of Cretaceous, Cenozoic, and historic oblique strike-slip motion along the Hines Creek fault is an open-ended question and not fully addressed by this study, and thus it persists as a major problem in Alaskan tectonics.

Yakutat Flat Slab Subduction and Oligocene to Present Alaska Range Exhumation History

The Yakutat microplate is a 15–30-km-thick oceanic plateau that is currently subducting under southern Alaska (Worthington et al., 2012). The subducted Yakutat slab extends for ~250 km northwestward beneath Alaska at a subduction angle of ~6° before the dip angle increases to ~20° and reaches a depth of 150 km beneath the Alaska Range, which is >600 km inboard of the Aleutian trench (Fig. 1; Eberhart-Phillips et al., 2006; Terhune et al., 2019). Hence, the Yakutat slab is highly coupled at the subduction margin and currently pushes southern Alaska generally to the north (Elliott and Freymueller, 2020).

The ca. 30 Ma initiation of the Wrangell arc (Brueseke et al., 2019; Berkelhammer et al., 2019) was coeval with the cessation of plutonism in the Alaska Range arc (Fig. 3; Jones et al., 2021; Regan et al., in 2021) and at ca. 25 Ma was followed by the cessation of Alaska Range dike emplacement (Trop et al., 2019). These magmatic events and hiatuses are interpreted to reflect the arrival of the Yakutat flat slab under southern Alaska (Trop et al., 2019; Jones et al., 2021). Another major plate boundary change occurred at 25 Ma, when the Pacific plate vector relative to North America underwent counter-clockwise rotation and increased in velocity (Jicha et al., 2018), resulting in a high magnitude of oblique convergence across the Denali fault system as southern Alaska moved to the northwest (Fig. 1). An additional 18° counter-clockwise rotation in convergence angle between the Pacific and Yakutat plates relative to North America at ca. 6 Ma further increased the northwestward-directed motion of southern Alaska (Engebretson et al., 1985; Doubrovine and Tarduno, 2008), resulting in the partitioning of slip onto the Totschunda fault (Allen et al., 2022) and increased orogenesis in the Alaska Range (Fitzgerald et al., 1993). Additionally, the 3-D numerical models of Jadamec et al. (2013) require strong coupling (i.e., a relatively high-viscosity shear zone) between a subducting slab and the overriding plate, in addition to the lithospheric-scale vertical weak zone, to replicate the block motion in southern Alaska observed between the subduction plate boundary and the Denali fault.

Basin analysis and geomorphic studies on both sides of the Alaska Range demonstrate that the region has been deforming and unroofing since ca. 29 Ma to present (Ridgway et al., 2007; Waldien et al., 2018; Trop et al., 2019). A broad range of thermochronological research has constrained the initial timing of exhumation and uplift of the topographically high modern Alaska Range and the Kluane Ranges of the Yukon (Fig. 1) to ca. 30–25 Ma (Benowitz et al., 2011a, 2012, 2014, 2019; Riccio et al., 2014; Burkett et al., 2016; Lease et al., 2016; McDermott et al., 2019, 2021; Waldien et al., 2021b, 2022). Together,

these thermochronological studies outline a history of asymmetrical uplift and unroofing of the Alaska Range through time and space along the Denali fault system, with juxtaposed crustal blocks being translated hundreds of kilometers and at times in and out of geometric complexities (Waldien et al., 2021a). Hence, counter to what has been suggested (Lease et al., 2016), there is no systematic evidence of orogen-scale, west-to-east deformation expansion in the Alaska Range. The pre-30 Ma history of the Alaska Range is less well-constrained, yet published thermochronology suggests a ca. 45 Ma increase in exhumation rates concomitant with a change in Pacific Plate convergence angle to more orthogonal (Doubrovine and Tarduno, 2008; Riccio et al., 2014; Lease et al., 2016).

The high peak region of the Hayes Range, our region of focus, is located at the apex of the arcuate Denali fault system and sandwiched between this lithospheric structure to the south and the Hines Creek fault to the north. Both east and west of the apex on the north side of the Mount Hayes restraining bend, orthogneiss, paragneiss, and schistose rocks yield 15–19 Ma ⁴⁰Ar/³⁹Ar muscovite and biotite ages that are inferred in places to reflect at least 14 km of Neogene exhumation (Benowitz et al., 2011a, 2014, 2019). These are the youngest ⁴⁰Ar/³⁹Ar mica ages along the entire Denali fault system. Peak elevations decrease (<1800 m) to the west of the Nenana Glacier area (Fig. 4), coinciding with an increase in rock cooling ages that indicates reduced long-term exhumation rates (Benowitz et al., 2011a; Perry, 2014).

In this study of the Hayes Range, we apply thermochronology to evaluate: (1) if and how the Hines Creek fault and Denali fault worked in tandem to facilitate the deep exhumation along the north side of the Mount Hayes restraining bend and associated uplift of the Hayes Range; (2) if the Between the Hines Creek and Denali faults block on the north side of the Mount Hayes restraining bend has been in prolonged, lateral fixed position relative to the bend; (3) if the high peak region of the Hayes Range has experienced south-side-up tilting; and (4) the potential for long-term localization of the Denali fault as a narrow fault zone.

METHODS

U-Pb Zircon Bedrock and Detrital Geochronology

We performed single-grain, U-Pb zircon geochronology using laser ablation-inductively coupled plasma–mass spectrometry (LA-ICP-MS) on two granitoid samples (n = 35 single grain analyses each) and one glacial outwash sample (n = 100 single grain analyses) to complement existing zircon U-Pb geochronological data sets (Figs. 3, S1, S2, and S3A; Tables S1 and S2¹) with three primary goals: (1) to constrain the magmatic history of the Hayes Range;

^{&#}x27;Supplemental Material. Includes new and legacy geochronology and thermochronology data. Analytical and thermal modeling details and methods are also included. Please visit https://doi.org/10.1130/GEOS.S.19067528 to access the supplemental material, and contact editing@geosociety.org with any questions.

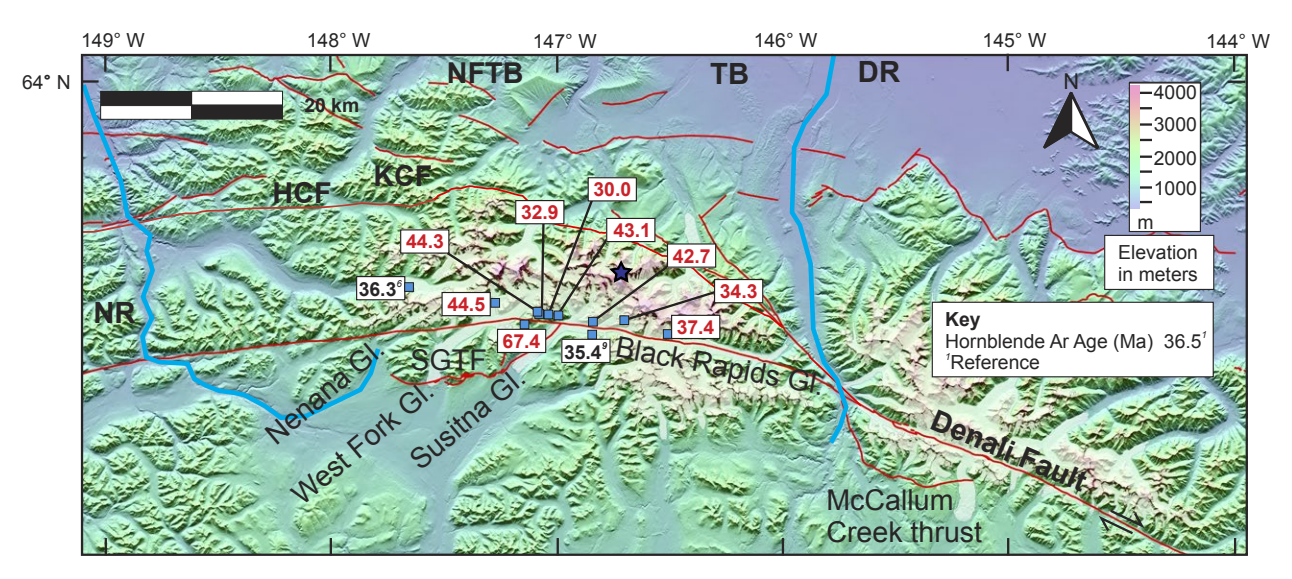


Figure 4. Digital elevation model depicts the high peak region of the eastern Alaska Range (U.S. Geological Survey Shuttle Radar Topography Mission, 30 m) with sample locations and 40Ar/39Ar hornblende ages from new (red) and published (black) bedrock samples north and south of the Denali fault. HCF—Hines Creek fault, KCF—Kansas Creek fault, SGTF—Susitna Glacier thrust fault, TB—Tanana basin, NFTB—Northern Foothills thrust belt, DR—Delta River, NR—Nenana River. Blue star is location of Mount Hayes. Sample references: 'Regan et al. (2021); 'Csejtey et al. (1992); 'Benowitz et al. (2011a).

(2) to provide a complimentary radiometric system to the new detrital glacial outwash ⁴⁰Ar/³⁹Ar biotite data set (Fig. S1); and (3) to better distinguish post-emplacement cooling versus exhumation and metamorphism-related cooling for the entirety of the thermochronological data sets. Detrital zircon (DZ) U-Pb data from modern rivers is especially important in this region because of the extensive snow and ice coverage of the Range (Fig. 2). LA-ICP-MS U-Pb geochronology of zircon was conducted at the Arizona LaserChron Center (ALC) (Gehrels et al., 2006, 2008; Gehrels and Pecha, 2014). The analyses involve ablation of zircon with a Photon Machines Analyte G2 excimer laser equipped with a HelEx ablation cell using a core spot diameter of 20 μm. See Table S1 for further details of the U-Pb dating.

⁴⁰Ar/³⁹Ar Geochronology and Thermochronology

Three modern glacial outwash sediment samples were analyzed with 40 Ar/ 39 Ar biotite single grain fusion experiments (~100 grains per sample; Fig. S1). Nine hornblende, 39 biotite, and seven potassium feldspar (K-feldspar) separates from 50 bedrock samples were analyzed using 40 Ar/ 39 Ar incremental step-heating experiments (Figs. 4–7). These results were combined with existing 40 Ar/ 39 Ar and K-Ar data sets (Figs. 5–7 and Tables S1 and S2) to: (1) evaluate if sub-glacial biotite sources provide different (younger) age populations than

exposed bedrock sources, and (2) better constrain patterns of rock cooling in the Hayes Range nominally between 500 °C and 150 °C (Reiners et al., 2005).

⁴⁰Ar/³⁹Ar geochronology and thermochronology were performed at the Geochronology Facility, University of Alaska Fairbanks, USA. Samples were crushed, sieved for the 250–1000 mm grain size, washed, put through heavy liquids, and then separated using magnetic and handpicking mineral separation techniques. Samples were analyzed on a VG-3600 MS using laser step-heating techniques described in Benowitz et al. (2014). Dating multiple minerals in the same sample provides information about a rock's thermal history from 500 °C to 150 °C. Whole-rock volcanic ages provide information about the timing of magmatism and dike emplacement. For a more detailed description of the ⁴⁰Ar/³⁹Ar analytical methods used and how uncertainties were derived, see the Supplemental Materials (Figs. S4–S6; Table S1 and Text S1, see footnote 1).

The K-feldspar age spectra are interpreted using multi-domain diffusion modeling (Lovera et al., 2002) to understand their thermal histories. Instead of performing diffusion experiments, we look at the timing of closure of the high-temperature (KFAT_{max}: ~350 °C; K-feldspar argon thermochronology) and low-temperature (KFAT_{min}: ~150 °C) domains for K-feldspar (Benowitz et al., 2014; Löbens et al., 2017). A summary of the 40 Ar/ 39 Ar results is given in Tables S1 and S2, with all ages quoted to \pm 1 σ and calculated using the constants of Renne et al. (2010). For detailed isotopic tables and figures, see the Supplemental Materials (Table S1 and Figs. S4–S6).

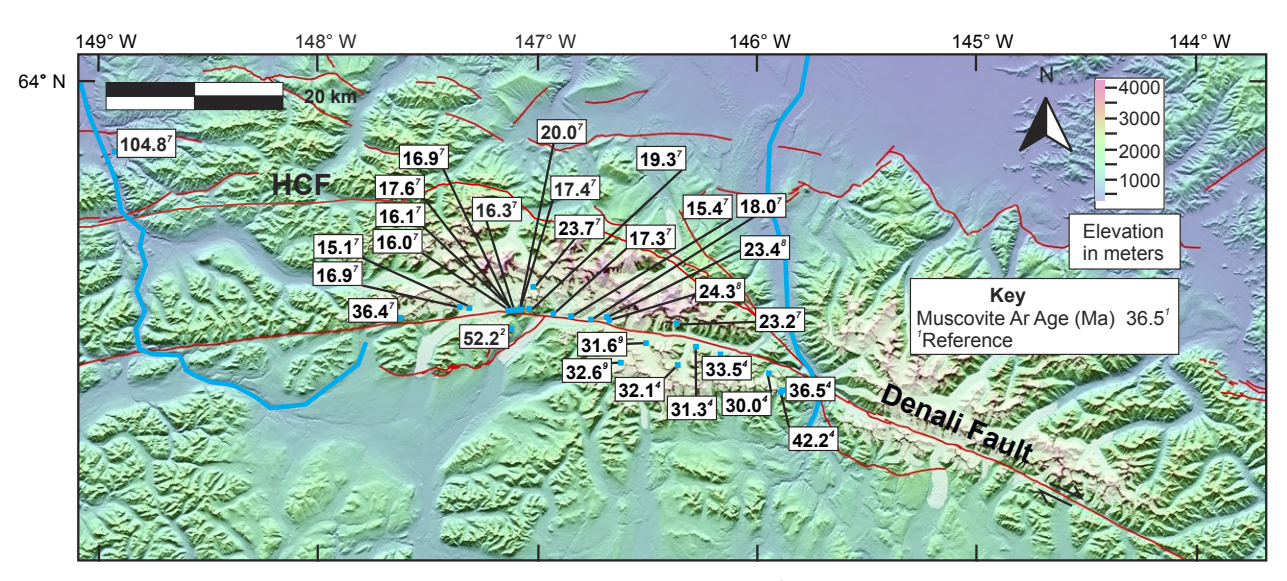


Figure 5. Digital elevation model depicts the high peak region of the eastern Alaska Range (U.S. Geological Survey Shuttle Radar Topography Mission, 30 m). Sample locations and integrated ⁴⁰Ar/³⁹Ar muscovite ages from published bedrock samples north and south of the Denali fault are shown. HCF—Hines Creek fault. Sample references: ¹Regan et al. (2021); ²Riccio et al. (2014); ⁴Nokleberg et al. (1992); ³Benowitz et al. (2019); ³Benowitz et al. (2011a).

Apatite Fission Track Thermochronology

We performed apatite fission track (AFT) analyses at the GeoSep Services facilities in Moscow, Idaho, USA, on 11 bedrock samples integrated with existing AFT data (Fig. 8) to (1) constrain regional rock cooling patterns between 120 °C and 60 °C, and (2) discern if the Hines Creek fault was an active structure during the Miocene–Pliocene. AFT age information is reported in Table S2, and AFT analytical data are reported in Table S1. For a detailed description of the methods used and how uncertainties were derived, see the Supplemental Materials (Text S2; see footnote 1).

Under typical continental geothermal gradients (20–30 °C), AFT thermochronology provides information about the thermal history of a rock sample in the upper ~3–5 km of the crust (Dodson, 1973). This technique involves analysis of the damage tracks formed by the spontaneous fission of ²³⁸U (Tagami and O'Sullivan, 2005). Depending on the apatite grain composition and cooling rate, fission tracks will partially anneal at temperatures >60 °C and completely anneal at temperatures >120 °C. This temperature window is referred to as the partial annealing zone. The temperature sensitivity of fission tracks allows for analysis of a rock sample's thermal history by measuring track lengths; shorter tracks indicate a longer residence time in the partial annealing zone (120–60 °C) and a relatively slower cooling rate (Donelick et al., 2005). Track-length distributions that include both long and partially annealed tracks indicate more complex thermal histories.

Apatite (U-Th)/He Thermochronology

Apatite (U-Th)/He (AHe) thermochronological analysis was performed by Jim Metcalf at the TRACK facilities in Boulder, Colorado, USA, on four samples (four to seven grains for each rock sample) integrated with published AHe data (Fig. 8) to (1) constrain regional rock cooling patterns between 80 °C and 40 °C, and (2) discern if the Hines Creek fault was an active structure during the Miocene–Pliocene.

(U-Th)/He thermochronology involves the analysis of alpha particles (⁴He) that accumulated in a mineral due to the radioactive decay of uranium and thorium (Reiners and Brandon, 2006). With a nominal closure temperature of 40–80 °C, AHe thermochronology provides information about the thermal history of a rock sample in the upper ~2–4 km of the crust (Farley, 2002). ⁴He particles travel ~20 mm from their parent atoms during radioactive decay, resulting in the ejection of ⁴He produced near the edge of a grain that requires corrections referred to as the Ft correction (Farley et al., 1996; Ketcham, 2005). The closure temperature of an apatite grain should vary depending on the grain size, cooling rate, and radiation damage that accumulated in the crystal lattice and should be reflected in intra-sample and overall grain age dispersion (Reiners and Farley, 2001; Flowers et al., 2009). However, closure temperature in individual apatite grains is often not clearly controlled by these kinetic factors (Fitzgerald et al., 2006).

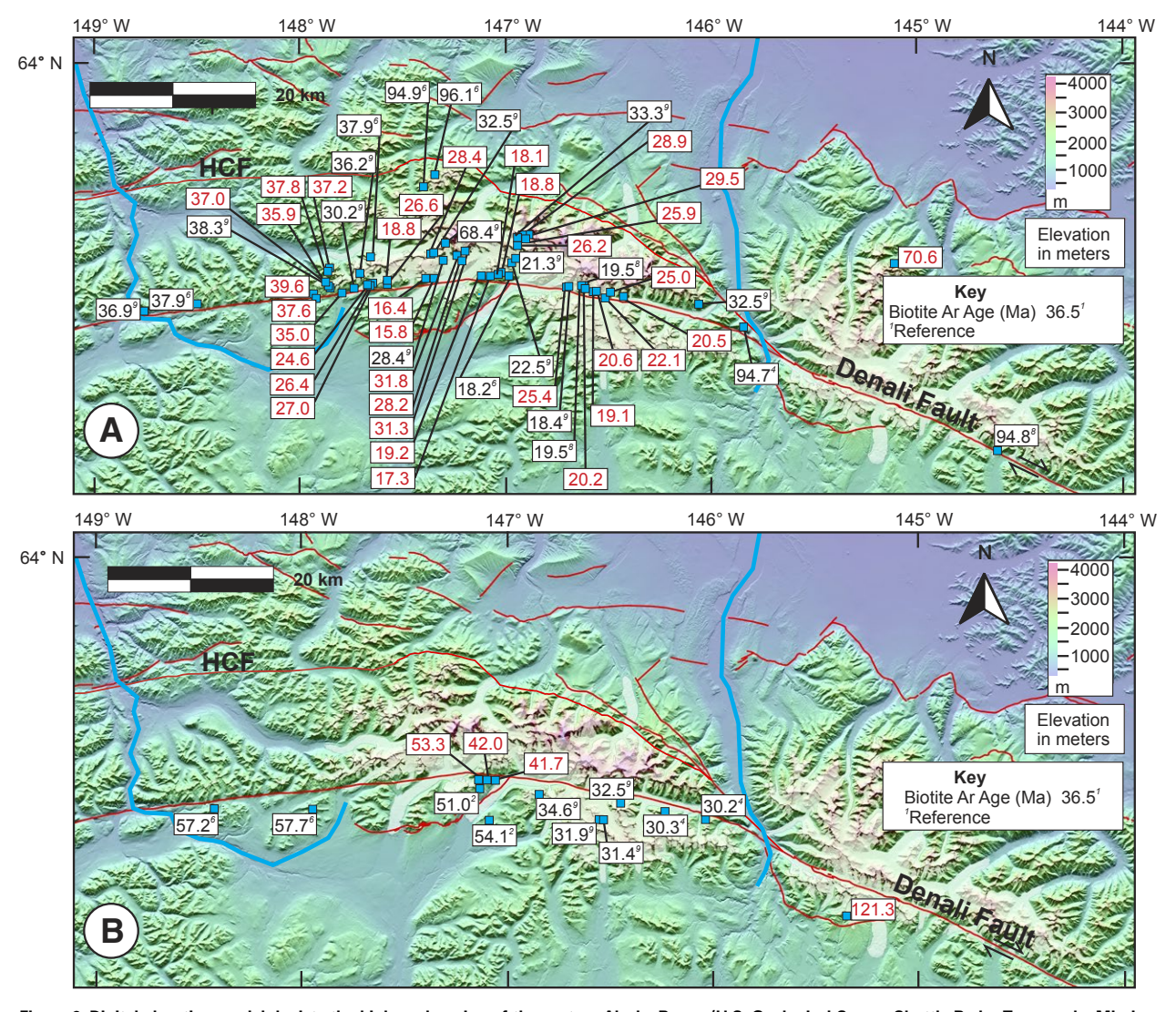


Figure 6. Digital elevation model depicts the high peak region of the eastern Alaska Range (U.S. Geological Survey Shuttle Radar Topography Mission, 30 m). (A) Sample locations and 40Ar/33Ar biotite ages from new (red) and published bedrock samples north of the Denali fault. (B) Sample locations and 40Ar/33Ar biotite ages from new (red) and published (black) bedrock samples south of the Denali fault. HCF—Hines Creek fault. Sample references: ¹Regan et al. (2021); ²Riccio et al. (2014); ⁴Nokleberg et al. (1992); °Csejtey et al. (1992); ³Benowitz et al. (2014); ³Benowitz et al. (2011a).

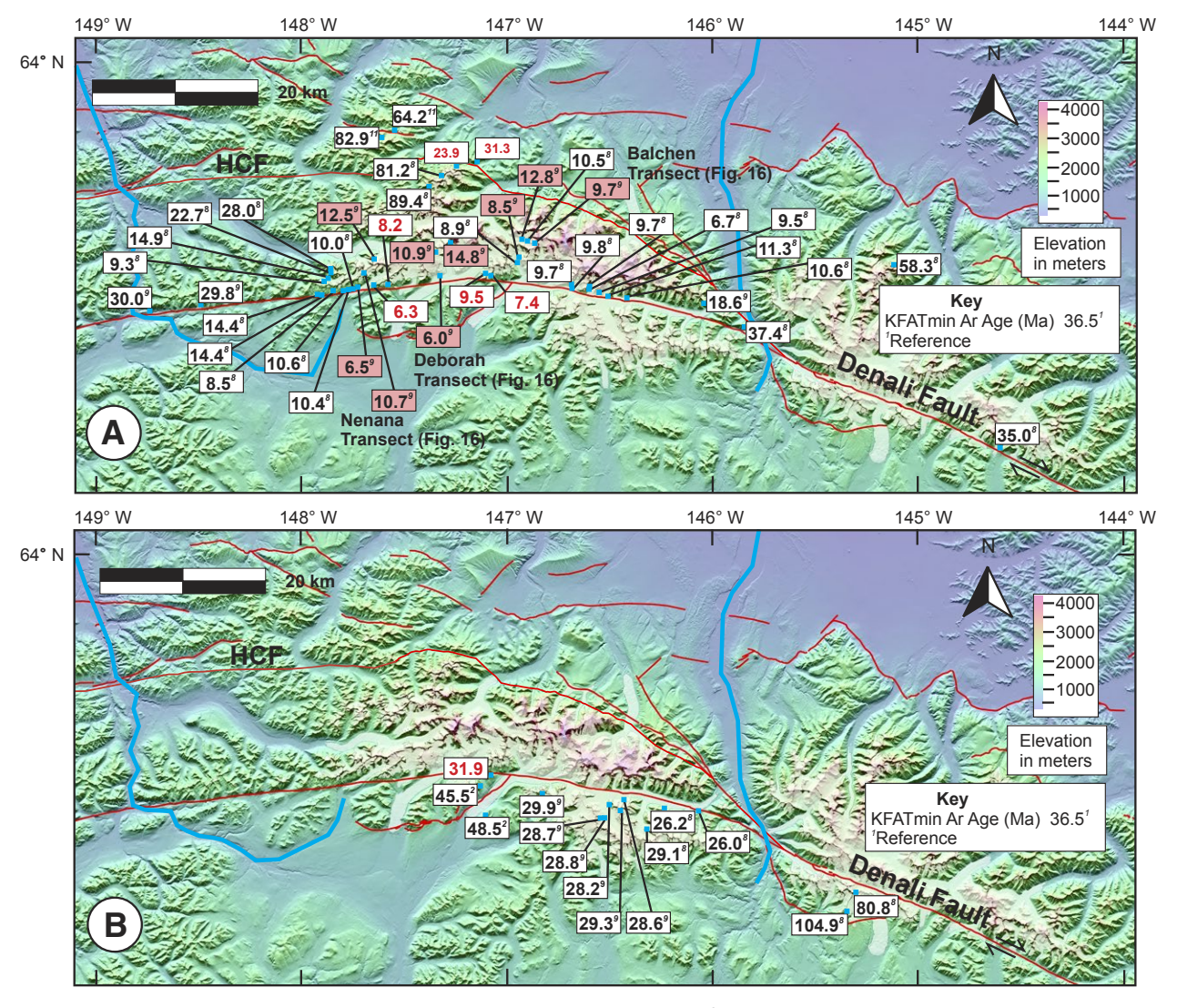


Figure 7. Digital elevation model depicts the high peak region of the eastern Alaska Range (U.S. Geological Survey Shuttle Radar Topography Mission, 30 m). (A) Sample locations and "Ar/13"Ar KFAT_{min} ages from new (red, Ma) and published (black, Ma) bedrock samples north of the Denali fault. (B) Sample locations and "Ar/3"Ar KFAT_{min} ages from new (red, Ma) and published (black, Ma) bedrock samples south of the Denali fault. Mauve data labels are the KFAT_{min} data plotted on the thermochronology transects on Figure 16. Abbreviations: HCF—Hines Creek fault. Sample references: 'Regan et al. (2021); 'Renowitz et al. (2014); 'Benowitz et al. (2011a); 'Benowitz et al. (2011b).

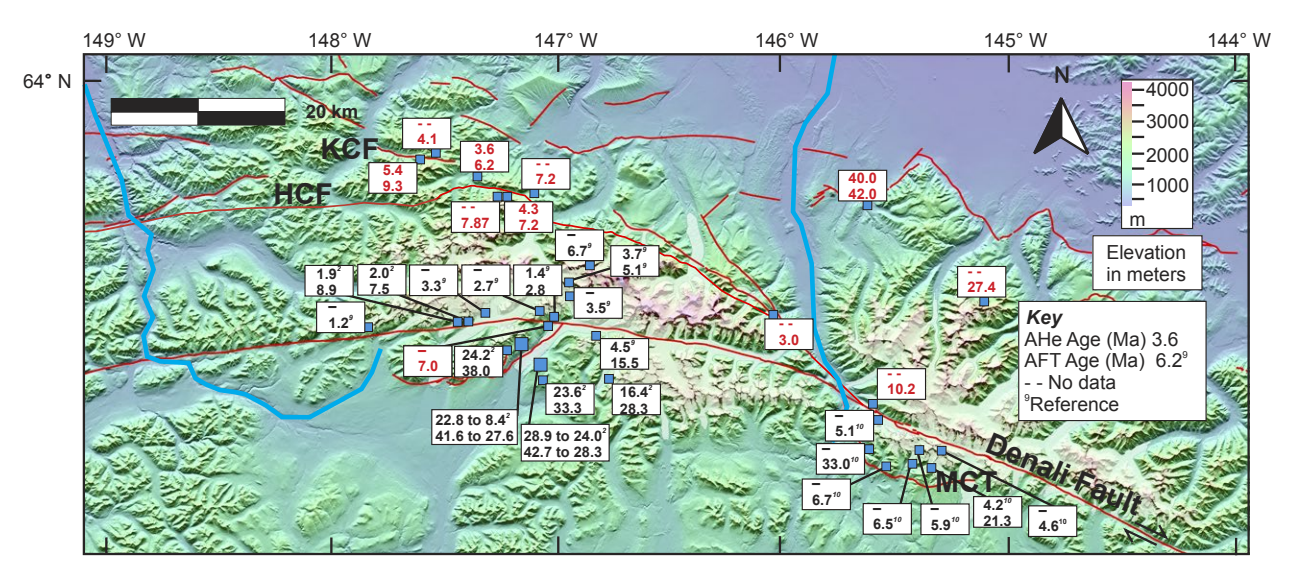


Figure 8. Digital elevation model of the high peak region of the eastern Alaska Range (U.S. Geological Survey Shuttle Radar Topography Mission, 30 m). Sample locations and AFT and AHe cooling ages are from new (red, Ma) and published (black, Ma) bedrock samples north and south of the Denali fault. HCF—Hines Creek fault, KCF—Kansas Creek fault, MCT—McCallum Creek thrust. Sample references: ²Riccio et al. (2014); ⁹Benowitz et al. (2011a); ¹⁰Waldien et al. (2018).

Corrections based on grain size (Ft) were applied to raw ages to correct for alpha particle ejection effects (Farley, 2002). Single-grain outliers, which were significantly older or younger than the mean age of grains in a sample, were found in three analyses. In general, this was due to low concentrations of uranium or ⁴He in that particular grain. We excluded these outliers from our calculations for average age of the samples, and it did not affect our results or interpretations. Given the natural dispersion of intra-sample single grains in AHe ages, we calculated the standard deviation for each sample grain set and applied this as the best approximation of the geologic error for the analysis (Spotila and Berger, 2010). Sample AHe average ages, uncertainties, and analytical data are reported in Table S1. For a more detailed description of the AHe methods used and how uncertainties were derived, see the Supplemental Materials (Text S3; see footnote 1).

HeFTy Thermal Modeling

Inverse thermal models were created for each of our samples using the HeFTy software program (Ketcham, 2005). Using an estimate of the annual present-day surface temperature (0 °C) and higher temperature (40Ar/39Ar) thermochronological data as constraints when available, HeFTy models the time and temperature

cooling history of a sample. The program evaluates "best-fit" cooling paths and slopes based on input age and AFT track-length constraints. We present Monte Carlo method inverse models showing acceptable and good cooling paths constrained in envelopes and weighted mean T-t paths after 200,000 runs. Input constraints for the models include 40 Ar/39 Ar K-feldspar ages (350–150 °C; Lovera et al., 2002), AFT data (120–60 °C; Reiners et al., 2005; single-grain ages, Dpar, track lengths, and angle of tracks to the c-axis), and average AHe ages. We use a broad temperature window (80–40 °C; Farley, 2002) for average AHe ages of samples because intra-sample grain age dispersal and overall grain age dispersal were not correlated with either grain size or effective uranium except for in sample 01JAR (Fig. S7 and Table S1, see footnote 1). Given the overlapping age of AHe grains and the AFT data, HeFTy was not able find good thermal paths for sample 01JAR when both AFT and AHe data sets were considered. Text S4 (see footnote 1) provides additional details on the HeFTy modeling.

RESULTS

Throughout this section we report new results compiled with previously published results (see Table S1 for data source references). This is the first publication to: (1) compile all U-Pb zircon and 40Ar/39Ar geochronology data

from the high peak region of the Hayes Range (which is complemented by select K-Ar data collected within 5 km of the Denali fault), and (2) evaluate temporal-spatial rock cooling patterns in relation to the position of the Hayes Range between the Hines Creek and Denali faults along the north side of the apex of the Mount Hayes restraining bend (Figs. 1 and 9–11).

U-Pb Zircon Results

Plutons in the Hayes Range vary in age from 97.5 ± 0.5 Ma (sample 02WIN) to 36.54 ± 0.6 Ma (sample 01PAN) on the north side of the Denali fault (Figs. 3 and 11A; Tables S1 and S2). On the south side of the Denali fault, plutons range in age from 98.1 ± 0.7 Ma (sample EAR10–24) to 32.6 ± 0.5 Ma (sample 098AP). On the north side of the Denali fault, no plutonic rock younger than 098 Ma has been identified east of Nenana Glacier aside from a small leuco-orthogneiss body (098, Sample 098) (Fig. 098; Tables S1 and S2). The modern catchment DZ data from the five glaciers draining the Denali fault trench in the Hayes Range provide similar overlapping age ranges as the bedrock data set with the addition of 098 grains older than ca. 098 Ma (Figs. 098, 098), Notably, the West Fork glacial outwash DZ age data do not contain ca. 0980 Ma zircons, which supports the U-Pb zircon bedrock evidence that the late Eocene magmatic event was minor in the deeply exhumed region of the Between the Hines Creek and Denali faults block (Benowitz et al., 098).

40Ar/39Ar Results

Hornblende

 $^{40}\text{Ar}/^{39}\text{Ar}$ hornblende ages from south of the Denali fault (35.4 \pm 0.6 Ma; sample 72ASt311) overlap with a major period of plutonism south of the fault (36.2 \pm 0.4 Ma, U-Pb zircon, sample 97SUS; Fig. 4). A K-Ar hornblende age north of the Denali fault in the Nenana Pluton (39.6 \pm 1.1 Ma, sample DT72–45A) overlaps with the U-Pb zircon age in the area (38.2 \pm 0.2 Ma, sample 37NEN). East of the Nenana Glacier area and north of the apex of the Mount Hayes restraining bend, $^{40}\text{Ar}/^{39}\text{Ar}$ hornblende ages range from ca. 45 Ma to 30 Ma (Fig. 4) and are significantly younger than U-Pb zircon ages from the same rocks and other proximal samples (ca. 95 Ma to 52 Ma; Figs. 3 and 9).

Muscovite, Biotite, and KFAT Ages

There is a clear contrast in K-Ar and 40 Ar/ 39 Ar muscovite, biotite, and K-feldspar ages across the Denali fault (Figs. 5–11) as described in detail by Benowitz et al. (2011a, 2014). To the south, the youngest muscovite (29.9 ± 0.8 Ma), biotite (30.2 ± 0.9 Ma), and KFAT_{min} (26.0 ± 0.2 Ma) ages are all from sample 71AWR480 (Table S2) and are significantly older than corresponding mineral phase K-Ar and 40 Ar/ 39 Ar cooling ages to the north of the Denali fault (Fig. 11).

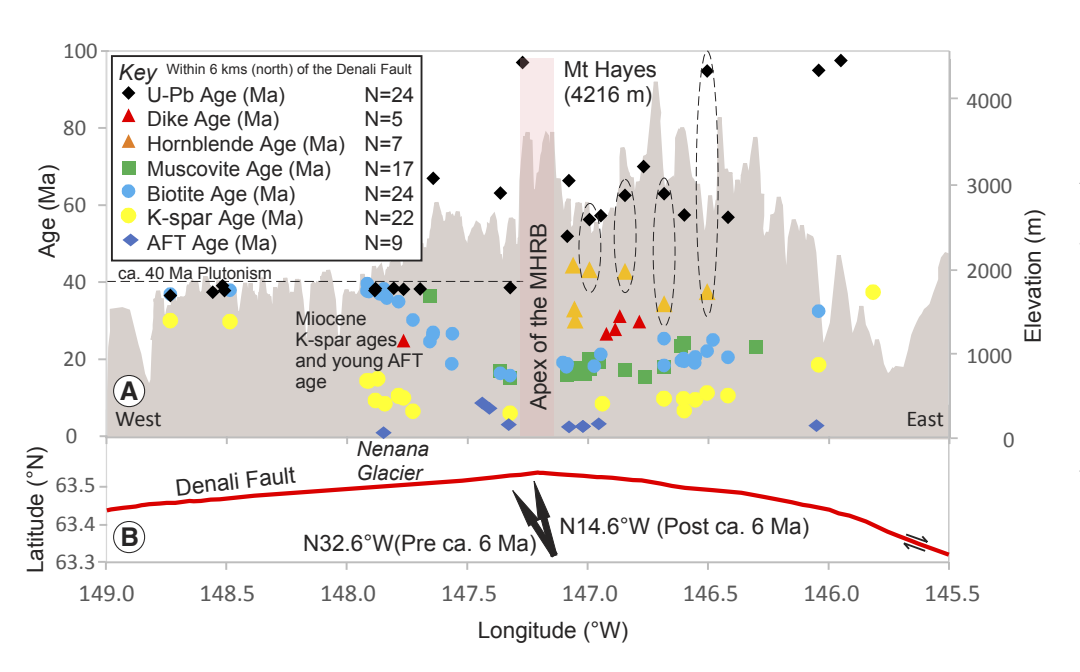


Figure 9. (A) Topographic profile of the divide north of the Denali fault (right axis) is shown. U-Pb zircon crystallization ages, 40Ar/39Ar groundmass dike ages, and 40Ar/39Ar muscovite, biotite, KFATmin, and AFT cooling ages are from samples collected within 6 km of the north side of the Denali fault. The age of plutonism is significantly older than those of all ⁴⁰Ar/³⁹Ar cooling ages except in the Nenana Glacier area and to its west. There is no systematic evidence of resetting due to Eocene-Oligocene intrusions. Dashed ellipses are sample U-Pb zircon-hornblende pairs. The 40Ar/39Ar muscovite, biotite, and KFAT_{min} cooling ages show a general younging trend approaching the apex of the Mount Haves restraining bend from both east and west, but the lower temperature KFAT_{min} and AFT ages remain young in the lower topography Nenana Glacier area. (B) Trace of the Denali fault and Pacific-North America convergence angle pre and post the ca. 6 Ma plate vector change. Data plotted are new and previously published (Table S2, see text footnote 1). MHRB-Mount Hayes restraining bend.

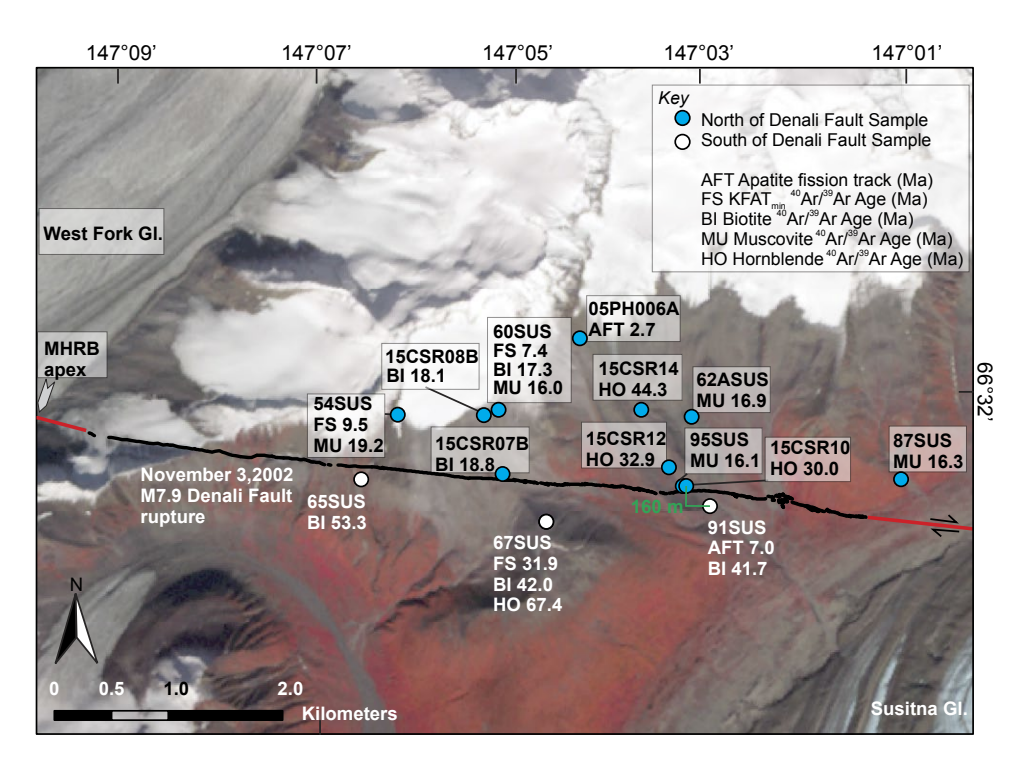


Figure 10. Thermochronological constraints on the width of the Denali fault at the apex of the Mount Hayes restraining bend are shown. The large contrast in cooling ages south and north of the Denali fault delineates a maximum width of 160 m for the fault's master strand. Data plotted are new and previously published (Table S2, see text footnote 1). Black-red line is the trace of the 2002 rupture reported in Haeussler (2009). MHRB—Mount Hayes restraining bend.

Cooling ages from sample 22DEB (Table S2) are strikingly young in the immediate (< 1 km north) vicinity of the Denali fault (40Ar/39Ar muscovite age of 15.1 \pm 0.9 Ma, biotite age of 15.8 \pm 0.2 Ma, and KFAT_{min} age of 6.0 \pm 0.2 Ma) and highlight a region of Miocene 40 Ar/39 Ar cooling ages within 8 km of and along the north side of the Mount Hayes restraining bend apex (Figs. 5-7). Muscovite and biotite 40Ar/39Ar cooling ages in this wedge get younger east to west toward the apex area of the Mount Hayes restraining bend and then get older than Miocene in the Nenana Glacier area (Fig. 9). KFAT_{min} ages remain young (6.5 ± 0.3 Ma, sample 32NEN; Table S2) in the Nenana Glacier region before getting progressively older to the west (28.4 ± 0.9 Ma, sample 322AST; Table S2). ⁴⁰Ar/³⁹Ar cooling ages increase with distance north of the Denali fault for all systems dated (Benowitz et al., 2011a). 40Ar/39Ar K-feldspar analysis of samples along the Hines Creek fault indicate protracted cooling through the Late Cretaceous (KFAT_{max}: 82.7 ± 1.6 Ma, sample 10ANK003; and 85.6 ± 0.5 Ma, sample 10ANK002) to the late Oligocene (KFAT_{min}: 23.9 ± 1.4 Ma, sample 10ANK003; and 31.3 \pm 1.2 Ma, sample 10ANK002) (Figs. 7 and Tables S1 and S2).

Detrital ⁴⁰Ar/³⁹Ar biotite ages from the modern Black Rapids, Susitna, and West Fork glacial outwash sediment samples produced generally similar cooling age ranges (18–82 Ma) and distribution as the corresponding bedrock sample ⁴⁰Ar/³⁹Ar biotite integrated age (K-Ar equivalent) compilations (Figs. 6,

11B, and S3B). Two grains from the detrital ⁴⁰Ar/³⁹Ar biotite data set were older than 82 Ma (103 Ma and 111 Ma; Table S1).

AFT, AHe, and HeFTy Thermal Modeling

Available AFT and AHe data from the Mount Hayes restraining bend are limited but demonstrate a trend of older ages on the south side (7.0 Ma AFT and 4.5 Ma AHe) than on the north side of the Mount Hayes restraining bend (1.2 Ma AFT, sample 05NEN; and 1.9 Ma AHe, sample EAR10–05) (Fig. 8), which is similar to the regional high temperature ⁴⁰Ar/³⁹Ar spatial patterns. The youngest AFT ages produced so far from the Hayes Range are from the Nenana Glacier Region. AFT and AHe cooling ages, similar to the ⁴⁰Ar/³⁹Ar cooling ages, get older northward from the Denali fault (Benowitz et al., 2011a).

The AFT and AHe ages from the Hines Creek and Kansas Creek faults (Fig. 8) appear to break the south–north pattern of older ages away from the Denali fault, with AFT ages as young as 4.1 Ma (sample LF196) and AHe ages as young as 3.6 Ma (sample 10ANK01). Late Miocene AFT cooling ages and Pliocene AHe cooling ages were produced from samples from the hanging wall and footwall of the Hines Creek and Kansas Creek faults (Fig. 8). AFT (27.4 Ma, sample 01HAJ)

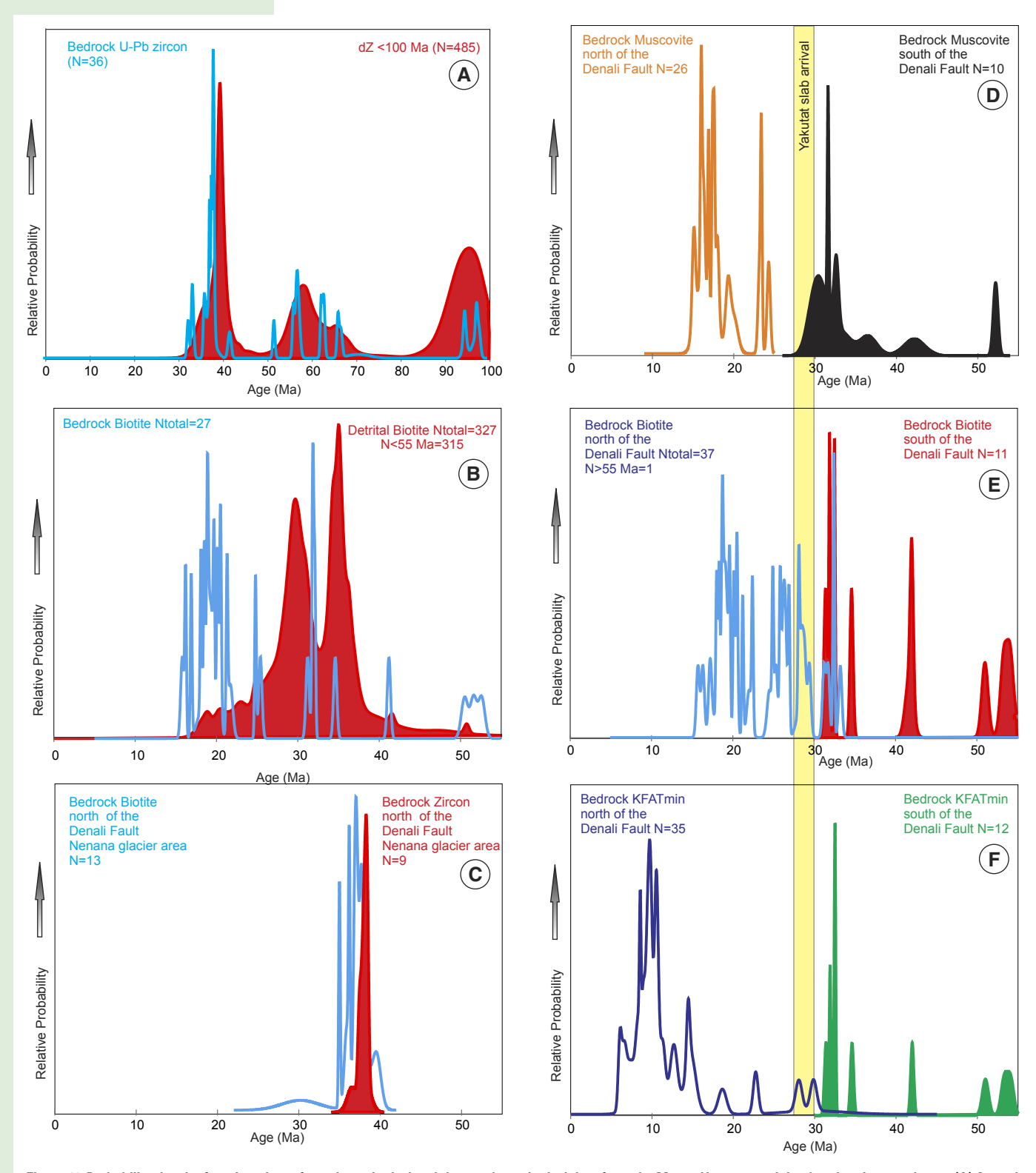


Figure 11. Probability density function plots of geochronological and thermochronological data from the Mount Hayes restraining bend region are shown. (A) Crystal-lization U-Pb ages from bedrock samples and detrital single grain U-Pb ages from glacial outwash samples <100 Ma (Figs. 3 and S3A; see text footnote 1). (B) Bedrock integrated and detrital **0Ar/**3Ar biotite ages <55 Ma (Figs. 6 and S3B; see text footnote 1). Ages from bedrock in the Nenana Glacier area are not included. (C) **0Ar/**3Ar biotite cooling ages and crystallization U-Pb zircon ages from bedrock samples from the Nenana Glacier area (Figs. 3 and 6). (D) Bedrock **0Ar/**3Ar muscovite ages north and south of the Denali fault (Fig. 5). (E) Bedrock **0Ar/**3Ar biotite ages north and south of the Denali fault (Fig. 7). Data plotted are new and previously published (Table S1, see text footnote 1).

and AHe (40.0 Ma, sample 01JAR) cooling ages and modeled cooling histories from samples collected from east of the Delta River and >30 km north of the Denali fault are older than cooling ages from the Mount Hayes restraining bend region and McCallum Creek thrust region (Figs. 8 and Table S1). HeFTy thermal modeling of samples collected along the Hines Creek demonstrate rapid cooling from the late Miocene onward (Figs. 12 and S7; see footnote 1). HeFTy thermal modeling of samples collected along the Kansas Creek fault also demonstrates rapid cooling from the late Miocene onward (Figs. 8 and S7).

Riccio et al. (2014) reported additional AFT and AHe ages from south of the Denali fault in the Mount Hayes restraining bend and primarily from the Susitna Glacier thrust fault region (AFT: Oligocene and AHe: Miocene cooling ages) (summarized in Fig. 8). New HeFTy kinetic modeling of the fission track analysis from sample 91SUS demonstrates rapid cooling of this sample at ca. 7 Ma (Fig. S7). This crustal block south of the Denali fault would have been 60–90 km to the east along a segment of the fault that experienced transpressional uplift during this time period (Waldien et al., 2018).

DISCUSSION

Hayes Range Magmatic History

There are no known plutons older than 100 Ma in the Hayes Range (Fig. 3); hence, the 59 DZ grains older than 100 Ma (Figs. 3, 11A, and S3A and

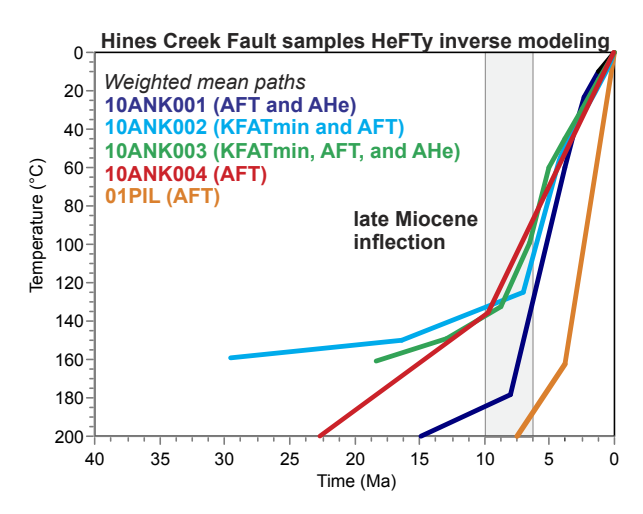


Figure 12. HeFTy (Ketcham, 2005) thermal models of samples collected along the Hines Creek fault (Fig. 8) show an increase in rock cooling rate and inferred exhumation during the late Miocene. Weighted mean paths and thermochronological systems applied are presented (e.g., AFT and AHe). Figure S7 and Text S4 provide additional HeFTy modeling details; see text footnote 1.

Table S1) are likely sourced from regional metasedimentary strata (Wilson et al., 2015) and/or reflect the systematic inaccuracy of ICP-MS U-Pb zircon dating (e.g., Herriott et al., 2019). The Hayes Range bedrock and detrital glacial outwash U-Pb data sets demonstrate periods of higher magmatic flux on both sides of the Denali fault at ca. 88–100 Ma, 58–70 Ma, and 32–42 Ma, which are separated by magmatic lulls (Figs. 3, 4, 11B, and 13). The similarity in age populations on both sides of the Denali fault illustrates the along-strike breadth of these magmatic belts given the minimum of 480 km of dextral slip since ca. 52 Ma (Waldien et al., 2021a) and ~305 km since ca. 33 Ma (Regan et al., 2021). Magmatism in the high peak region of the Hayes Range continued until at least ca. 25 Ma based on five dated mafic dikes that range in age from 32 Ma to 25 Ma (Figs. 9 and 13) (Trop et al., 2019). Lastly, at ca. 1 Ma there was a reinitialization of arc magmatism in the broader Hayes Range area (Figs. 1 and 13; Andronikov and Mukasa, 2010; Brueseke et al., 2021; Waldien et al., 2022).

We infer the ca. 95 Ma pulse of magmatism reflects arc magmatism during the accretion of Wrangellia with the North American margin, but this magmatic suite deserves further investigations of the petrogenesis to truly discern the tectonic setting responsible (Fig. 13; e.g., Manselle et al., 2020). Though there is limited geochemistry available (Regan et al., 2020, 2021), we infer that the pulses of magmatism at ca. 58–70 Ma and 32–42 Ma are related to arc magmatism given the overlap in ages with arc magmatism in the central Alaska Range (Trop et al., 2019). The hiatus from ca. 55–45 Ma has been proposed to be due to a slab window under much of southern Alaska during this time period (Cole et al., 2006; Benowitz et al., 2012; Terhune et al., 2019). Alaska Range arc plutonism ceased by ca. 30 Ma due to the initiation of Yakutat flat slab subduction (Figs. 1 and 13) (Lease et al., 2016; Jones et al., 2021; Regan et al., 2021).

The Alaska Range Suture Zone Localizes Arc Magmatism

A compilation of U-Pb zircon bedrock and DZ data from the western and central Alaska Range and the Hayes Range reveals overlapping periods of high magmatic flux at ca. 58 Ma and ca. 39 Ma over an east-to-west distance of ~480 km (Figs. 1 and 13; Table S1). The Wrangell arc initiated by 30 Ma to the southwest of the Hayes Range and coeval with the shutting down of the Alaska Range arc (Brueseke et al., 2019; Berkelhammer et al., 2019; Trop et al., 2022; Fig. 13).

The Alaska Range and Wrangell arcs were both emplaced into the broad suture zone between Wrangellia and the Yukon Tanana terrane (Fig. 1). Wrangell and Alaska Range arc magmatism occurred both adjacent to, and away from, the Denali, Hines Creek, Totschunda, and Duke River faults. Hence, these structures acting as magma conduits alone (e.g., Gómez-Vasconcelos et al., 2020) cannot explain Late Cretaceous to present localization of Alaska Range and Wrangell arc magmatism within and adjacent to the Wrangellia-North America suture zone.

The suture zone is defined by lithologic and thickness variations of the crust (Fitzgerald et al., 2014; Allam et al., 2017), including crustal thickness variations

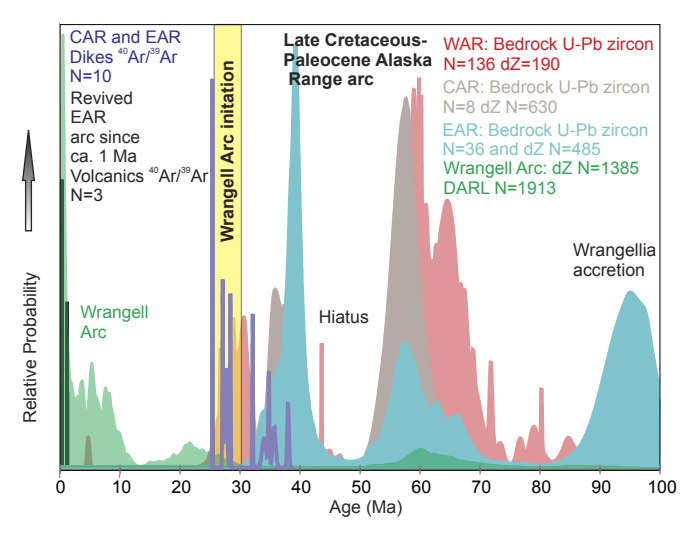


Figure 13. Compilation of bedrock U-Pb zircon crystallization and detrital U-Pb single grain zircon ages from modern river sediment in the Western, Central, and Eastern Alaska Range (Fig. 1) demonstrate similar periods of magmatic fluxes and hiatuses. The distance to the trench has varied over time but since at least 70 Ma, arc magmatism has been localized in the Alaska Range suture zone, which indicates that upper plate thickness heterogeneity is controlling the dip of the underlying slab through time and the reactivated suture zone faults are acting as magma conduits (Trop et al., 2019). Wrangell arc data are from Trop et al. (2022; DARL—detrital argon lithic grains); Western Alaska Range (WAR; Lease et al., 2016; Trop et al., 2019; Regan et al., 2020); Eastern Alaska Range (EAR; Athey et al., 2006; Andronikov and Mukasa, 2010; Trop et al., 2019; Regan et al., 2021; this study). Data details are in Table S1, see text footnote 1.

across the Denali, Hines, Totschunda, and Duke River faults (Fig. 1B). Given the evidence for sustained arc localization in the suture zone since ca. 70 Ma (Fig. 13), we posit that upper plate crustal thickness variations within the suture zone likely played a hydrostatic role in controlling the dip of the underlying slab(s) regardless of slab characteristics (Trop et al., 2019).

Cooling History South of the Mount Hayes Restraining Bend

There are no Miocene ⁴⁰Ar/³⁹Ar muscovite, biotite, or KFAT_{min} ages recorded in rocks from south of the Mount Hayes restraining bend (Figs. 5–7 and 10–11). Topography is also relatively subdued compared to that of the bend's north side (peak heights of 2479 m south versus 4216 m north of the bend). The presence of AFT cooling ages as young as ca. 7 Ma, AHe ages as young as ca. 4.5 Ma (Fig. 8), and active reverse faults such as the Susitna Glacier thrust fault (Personius et al., 2017) indicate locally high rates of deformation since the

late Miocene. However, the transient nature of focused deformation along the south side of the arcuate Denali fault, as crustal blocks are translated through this long wavelength geometric complexity (Regan et al., 2021), likely contributes to the lack of deep Oligocene–Miocene exhumation south of this stable, gentle (13°) restraining bend.

Cooling History North of the Mount Hayes Restraining Bend

West of the Nenana Glacier area, hornblende and biotite ages approach known ca. 40 Ma magmatic ages (Fig. 9). As noted above, there are no ca. 40 Ma plutons east of sample 22DEB (38.6 Ma), and this pluton is likely of limited size given regional U-Pb zircon bedrock constraints and its absence in the DZ age spectra from the West Fork drainage (Figs. 3 and S3A). Moreover, from the West Fork area and to the east, there is no evidence that regional Cenozoic magmatism, plutons, or dikes reset or partially reset any of the mineral phases analyzed with ⁴⁰Ar/³⁹Ar, AFT, and AHe thermochronology in samples collected north of the Denali fault. Hence, we infer that the hornblende, muscovite, and biotite ⁴⁰Ar/³⁹Ar ages north of the Denali fault and west of the Nenana Glacier area all reflect cooling related to metamorphic recrystallization and/or exhumation. The KFAT_{min}, AFT, and AHe ages have closure temperatures that correspond to depths above the brittle-ductile transition and are inferred to reflect solely exhumation-related cooling of the Between the Hines Creek and Denali faults block.

The detrital ⁴⁰Ar/³⁹Ar biotite data set contains similar age populations as the bedrock ⁴⁰Ar/³⁹Ar biotite data set (Figs. 6, 11B, and S3B). Hence, if there is coupling between tectonics and glacial processes in the Hayes Range, it is from a recent feedback system (Benowitz et al., 2011a) and has not rejuvenated the ⁴⁰Ar/³⁹Ar biotite signal. The 12 detrital biotite grains that are older than 55 Ma are not reflected in bedrock ages and are likely sourced from regions south of the Denali fault that experienced minimal Cenozoic exhumation (Benowitz et al., 2011a).

Simple regressed cooling histories using nominal closure temperatures (Reiners et al., 2005) based on multi-thermochronometers from the same sample or neighboring samples within ~1 km of the Denali fault support the initiation of rock cooling and inferred deformation north of the Mount Hayes restraining bend by ca. 45 Ma and an apparent increase after ca. 30 Ma (Fig. 14 and Table S1). The rate of rock cooling from ca. 45 Ma to ca. 30 Ma is skewed upward by applying a closure temperature of 350 °C to most muscovite ⁴⁰Ar/³⁹Ar ages because of possible recrystallization at low temperatures. Recrystallization or neocrystallization of muscovite below its closure temperature (typically Tc of ~400 °C; Harrison et al., 2009) is inferred if ⁴⁰Ar/³⁹Ar biotite ages (typically Tc of 350 °C; Reiners et al., 2005) are older than muscovite from the same sample. Hence, the newly calculated post-30 Ma nominal rock cooling rates of 17 °C/m.y. from this region are slower than previously constrained (Benowitz et al., 2014).

The occurrence of Eocene–Oligocene Alaska Range rock cooling is not surprising given the Denali fault time-averaged, slip-rate history since ca. 52 Ma

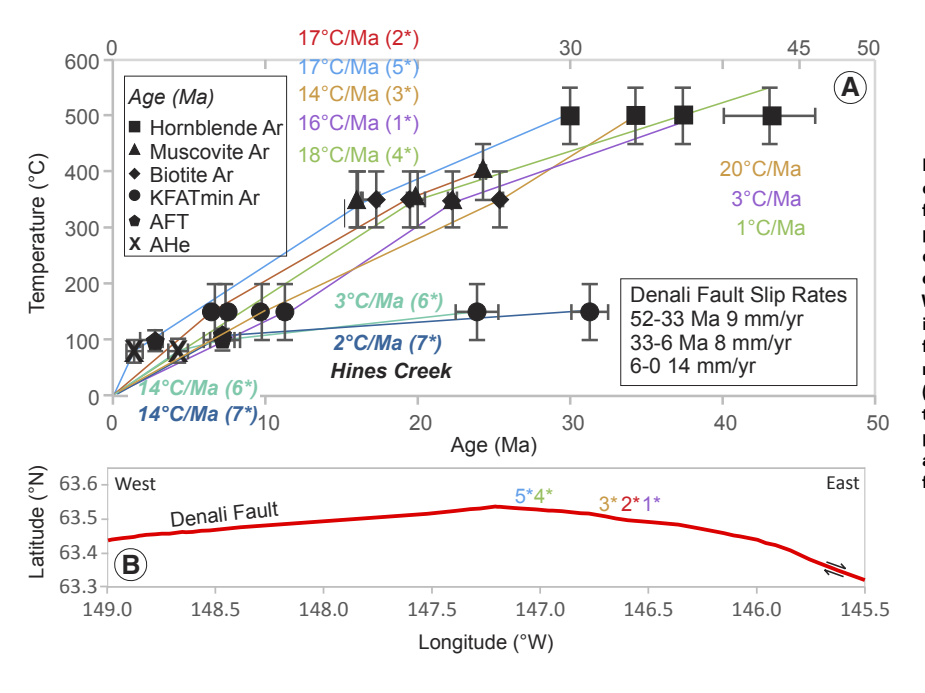


Figure 14. (A) Cooling curves are based on nominal closure temperatures for different mineral systems from intrasample and nearby (~1 km; set 5*) samples north of the Mount Hayes restraining bend; clustered locales are differentiated by different colors. Denali fault long-term average slip rates are from Waldien et al. (2021a). Rock cooling rates generally increase after ca. 30 Ma for samples along the Denali fault and after ca. 6 Ma for the samples collected near the Hines Creek fault. (B) General locations (e.g., 2*) along the Denali fault for samples used to construct the corresponding individual cooling paths in Figure 14A. Hines Creek sample locations are in Figure 8. Sample details in Table S1 (see text footnote 1).

(9 mm/yr; Waldien et al., 2021a) and other regional evidence of Eocene rock cooling along the Denali fault system (Benowitz et al., 2014; Caine et al., 2015; Lease et al., 2016). Given the generally slow rates of exhumation and inferred slip-partitioning along the Denali fault during the time period of ca. 52 Ma to 30 Ma, the fault's east-to-west slip gradient may have been less compared to after this time period (Regan et al., 2021). This tectonic scenario was proposed to have led to escape tectonics (Redfield et al., 2007).

The Hines Creek fault age data indicate slow rock cooling before an uptick to rapid cooling during the late Miocene (Figs. 12, 14, and S6). Although rock cooling was slower before the late Miocene along the Hines Creek fault, there is evidence from basin analysis and thermochronology that the fault was active throughout the Cenozoic (Nokleberg et al., 2013; this study). The ⁴⁰Ar/³⁹Ar down-stepping age spectrum from samples located near but across the Hines Creek fault from each other (10ANK02 and 10ANK03; Fig. S6) is similar and spans ca. 80 Ma to 30 Ma. AFT ages from the same samples are also similar at ca. 7 Ma (Fig. 8). An implication of across-fault, mirrored thermal histories of these samples suggests there likely was no significant strike-slip offset along the Hines Creek fault since at least ca. 80 Ma.

Along a fault-parallel transect from east to west on the north side of the Denali fault, ⁴⁰Ar/³⁹Ar muscovite and biotite ages get younger toward the Mount Hayes restraining bend apex before getting older toward the Nenana Glacier area to the west (Fig. 9). KFAT_{min} ages follow a similar pattern but stay young

in the Nenana Glacier area, unlike biotite cooling ages from the Nenana pluton that overlap the zircon U-Pb ages (ca. 40 Ma). The youngest AFT ages from the Hayes Range are also located in the Nenana Glacier area (Fig. 8). Benowitz et al. (2011a) interpreted this Mount Hayes restraining bend east-west cooling age pattern to reflect a migrating asperity along the south side of the Denali fault. With more data produced and compiled, we now favor a model where deformation had been focused along the Mount Hayes restraining bend apex and to the east from ca. 45 Ma to ca. 6 Ma and then the exhumation front expanded to include the Nenana Glacier area after ca. 6 Ma.

The increase in rock cooling rates at ca. 30 Ma was coeval with the initiation of Yakutat flat slab subduction (Figs. 11D–11F and 14). A tectonic event associated with a Pacific–North America plate vector change at ca. 25 Ma has also been suggested (Jicha et al., 2018; Berkelhammer et al., 2019; Trop et al., 2019), but our new data do not speak to this inferred increase in convergence across the Denali fault system. After the Pacific–North America plate vector change at ca. 6 Ma (Engebretson et al.,1985; Doubrovine and Tarduno, 2008), the region of focused exhumation in the Between the Hines Creek and Denali faults block broadened to include the Nenana Glacier area (Fig. 9). This late Miocene expansion of the region of focused exhumation explains why the biotite cooling ages immediately west of the Nenana Glacier area are generally similar to pluton crystallization ages in the region, but KFAT_{min} and AFT ages are some of the youngest in the Hayes Range. An AFT vertical

profile on a peak on the north side of Nenana Glacier shows a break in slope at ca. 6 Ma (Perry, 2014), which supports the interpretation that the region of rapid exhumation along the north side of the Mount Hayes restraining bend broadened at this time.

Due to preexisting curvature of the Mount Hayes restraining bend (Regan et al., 2021), there was a greater increase in convergence along the western limb of the bend with the change in obliquity at ca. 6 Ma than along the eastern limb of the bend. This expansion of the zone of rapid exhumation on the north side of the Mount Hayes restraining bend aligns with the ca. 6 Ma southern Alaska tectonic event (Fitzgerald et al., 1993; Waldien et al., 2018; Allen et al., 2022) that was also experienced in the Yukon Kluane Ranges (McDermott et al., 2021).

Age of the Mount Hayes Restraining Bend and the Arcuate Shape of the Denali Fault System

When and why the Denali fault became curved and whether the bend continues to tighten is a long-standing Alaskan tectonic-geomorphic question (e.g., Haeussler, 2008). Regan et al. (2021), through strain partitioning analysis, demonstrates that the arcuate shape of the Denali fault system was established by ca. 33 Ma. The ⁴⁰Ar/³⁹Ar hornblende (ca. 45–30 Ma), muscovite (ca. 24–15 Ma), and biotite (ca. 25–16 Ma) cooling ages combined with the KFAT_{min} ages (ca. 11–6 Ma), AFT ages (ca. 9–1 Ma), and AHe (ca. 5–1 Ma) ages within 6 km of the north side of the Denali fault indicate that the apex of the Mount Hayes restraining bend was established by and has been a persistent region of exhumation since at least ca. 45 Ma (Figs. 5–10). The metamorphic grade of the rocks in the region of peak exhumation decreases from amphibolite to upper greenschist facies to the west of the West Fork Glacier and decreases again across the Nenana glacier to very low-grade slate and unmetamorphosed shale (Brewer and Craddock, 1989; Csejtey et al., 1992).

No high-grade metamorphic rocks similar to those exposed on the north side of the Mount Hayes restraining bend exist on the south side of the Denali fault to the west, which indicates that the fault was not truncated and/or abandoned and moved north with respect to the region of exhumation since at least 45 Ma. Thus, we surmise, based on the long-lived cooling age patterns, that rocks north of the Denali fault and the Mount Hayes restraining bend are in a lateral fixed position relative to each other.

The Mount Hayes restraining bend apex appears to be acting as a focal point since ca. 45 Ma for the indention of southern Alaska against the Denali fault, which pushes the Hayes Range to the north (Figs. 9–10).

Paleomagnetic data on Late Cretaceous and early Cenozoic igneous rocks support the counterclockwise rotation of southern Alaska between ca. 68 Ma and 44 Ma (Thrupp and Coe, 1986; Hillhouse and Coe, 1994). Our new exhumation-related ca. 45 Ma to 30 Ma ⁴⁰Ar/³⁹Ar hornblende ages from the convex side of the apex of the arcuate Denali fault system, in combination with the Between the Hines Creek and Denali faults block thermochronological data set

in its entirety, indicate a broad scale, stable Denali fault geometry responding to changing stress fields through time. Hence, a bent Denali fault by ca. 45 Ma aligns with the southern Alaskan orocline hypothesis.

The gentle angle (13°) of the bend likely contributed to the stability of the bend as a long-lived geometric feature (Hatem et al., 2015), which shows no evidence for bend migration nor significant shape change since ca. 45 Ma and indicates that it is a fixed feature of the north side of the Denali fault. The master strand of the arcuate Denali fault is not only a long-lived stable feature but is also narrow. This interpretation is based on combining the cooling ages with macroscopic fabrics. Overall, the youngest amphibole and mica ages are within 1500 m of the Denali fault and coincide with orthogneiss, which has a consistent subvertical foliation parallel to the fault, oblique mineral lineations, and dextral kinematic indicators. This suggests that the highest strain part of the fault zone remained relatively narrow below the seismogenic zone to midcrustal depths (Figs. 3 and 5-6) (Roeske et al., 2011; Tait, 2017). Furthermore, the distance between sample 95SUS on the north side of the fault (40Ar/39Ar muscovite, ca. 16 Ma) and sample 91SUS south of the Denali fault (40Ar/39Ar biotite, ca. 42 Ma) is ~160 m, which provides a maximum width for the master strand of the Denali fault zone at this site (Fig. 10). These 40Ar/39Ar 95SUS and 91SUS results produced flat, undistributed age spectrum as did the mineral phases dated with the 40Ar/39Ar technique from the other samples from near the Denali fault, which are plotted in Figure 10. The lack of thermal disturbance, along with the low amount of hydrothermal alteration in the bedrock outside of the active fault trace damage zone, confirm that these samples are not from blocks entrapped in the fault zone. This set of north and south samples also brackets the trace of the 2002 M7.9 Denali fault rupture (Fig. 10). In summation, the KFAT, AFT, and AHe near-fault cooling age patterns document that the master strand is stable in the upper crust, and that same strand must connect vertically over an equally narrow zone below the brittle-plastic transition to produce the along- and across-strike cooling age patterns in the higher temperature 40Ar/39Ar hornblende, muscovite, and biotite systems.

Given that persistent rapid exhumation is known to vertically advect crustal isotherms (Braun et al., 2006), the Eocene–present rapid exhumation north of the Mount Hayes restraining bend would have contributed to thermal weakening of the upper crust near the fault and facilitated the observed localization of the Denali fault system as documented on the Alpine fault of New Zealand (e.g., Koons et al., 2003). The narrow span of both the brittle fault trace of the Denali fault and the mylonitic rocks adjacent to it on the north side (Roeske et al., 2011), combined with the stability of the Mount Hayes restraining bend and focused Eocene–Oligocene magmatism along the fault (Fig. 3), imply long-lived localization through the lithosphere. Waldien et al. (2021a) also reached this conclusion based on geological and geophysical evidence from south of the Denali fault and along the strike-length of the fault into the Yukon territory.

This conclusion is in contrast to the model of "orogenic float," a concept proposed for transpressional orogens that argues for a weak zone in the crust that detaches upper crustal structures from the lower crust–mantle region

(Oldow et al., 1990). The "float" or detachment model was proposed for active tectonic regions in the Yukon territory and Alaska (Mazzotti and Hyndman, 2002) in part based on geophysical evidence that the Moho appears to be relatively flat in the northern Canadian Cordillera. However, more dense seismic arrays deployed in the past 10 years indicate that some of the major active and inactive high-angle faults in Alaska and Yukon have offsets of the Moho directly below them (Brennan et al., 2011; Allam et al., 2017; Miller et al., 2018; Estève et al., 2020). We and others interpret the alignment of the surface trace of these faults and Moho offsets at depth to indicate that the surface expression of these faults corresponds with the geophysical expression at depth, and these faults are lithospheric in scale. In addition, numerical models of the Denali fault require it to be a subvertical zone of weakness through the lithosphere to produce the observed uplift along the fault, which supports the Denali fault being a zone of weakness (Jadamec et al., 2013).

The Denali fault zone is not only narrow in our region of study; it also appears to be in a narrow zone (10–35 m) along strike to the east, where focused exhumation is occurring in the Kluane Ranges of the Yukon (Caine et al., 2015, 2018; McDermott et al., 2021), and less than 100 m wide to the west in the Mount McKinley restraining bend (Benowitz et al., 2021). We propose that the rapid vertical tectonics environ of the Denali fault leads to beveling off of crustal material. Hence, the development of upper-crustal brittle fault splays is outpaced by erosion, and the master trace of the fault remains a narrow zone. Furthermore, the Denali fault has been in a convergent regime to varying degrees both through time and along the arcuate fault since at least ca. 45 Ma (Lease et al., 2016; this study). This compressive state likely also has contributed to the stability and localization of the Denali fault through time as proposed by Regan et al. (2021).

Between the Hines Creek and Denali Faults Block

Past work has focused on the stark contrast in cooling ages and amount of Oligocene-Neogene exhumation across the Denali fault in the Hayes Range, with deep (>14 km) Neogene exhumation only occurring on the north side of the Mount Hayes restraining bend compared to <5 km on the south side (Benowitz et al., 2011a, 2014, 2019; Riccio et al., 2014). Our compiled thermochronological data sets reinforce the striking contrast in cooling histories across the Denali fault. The data further highlight the paradox of persistent deformation being focused on the outside side of the Mount Hayes restraining bend. Based on thermochronology (this study), seismicity (Eberhart-Phillips et al., 2003; Koehler et al., 2012), and stratigraphic constraints (Ridgway et al., 2007; Nokleberg et al., 2013), both the Hines Creek and Denali faults have been active since at least ca. 45 Ma as structures with a component of dip-slip motion. We propose that a component of the convergence across the Denali fault is taken up through vertical extrusion of the Between the Hines Creek and Denali faults block along the weak Hines Creek and Denali fault displacement free faces (Fig. 15).

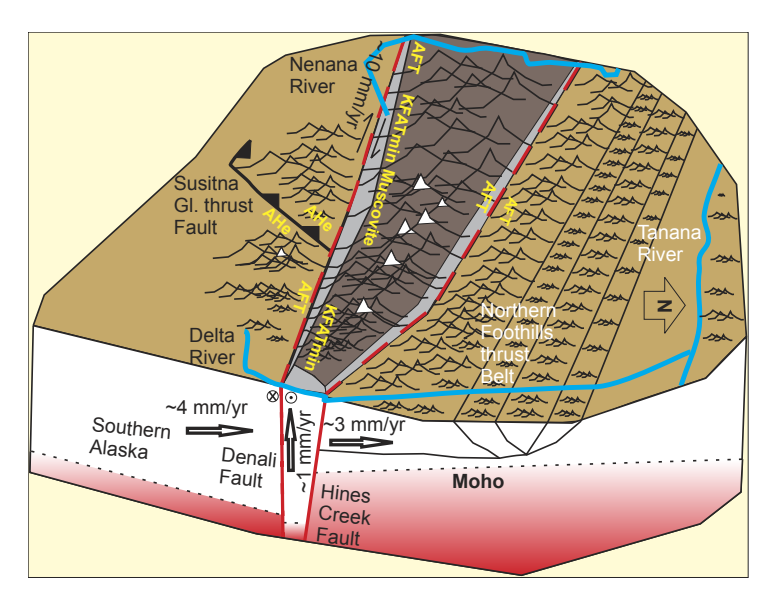


Figure 15. Schematic shows vertical extrusion (gray panels) of the Between the Hines Creek and Denali faults block (dark brown). Exhumation through different thermochronological systems since the Miocene is annotated in yellow text (e.g., Miocene cooling ages reflect exhumation deep enough to exhume rocks with Miocene muscovite cooling ages). Convergence rates are from Ellott and Freymueller (2020) and Bemis et al. (2015), and Denali fault slip rate is from Haeussler et al. (2017). Denali and Hines Creek Moho offsets and crustal thickness variation are from Veenstra et al. (2006), Brennan et al. (2011), and Allam et al. (2017). White capped peaks represent highly glaciated topography. AFT—apatite fission track.

The existence of an independent Between the Hines Creek and Denali faults block is supported by geodetic modeling (Elliott and Freymueller, 2020). Modeled fault-normal convergence between southern Alaska and the Between the Hines Creek and Denali faults block along the west side of the apex of the Mount Hayes restraining bend is ~4 mm/yr and oriented almost due north (Figs. 1 and 15). This convergence is pushing the Between the Hines Creek and Denali faults block to the north, which is accommodated in part by deformation on structures subparallel to the Denali fault in the Northern Foothills thrust belt (Bemis and Wallace, 2007, 2012, 2015).

Bemis et al. (2015) calculated a shortening rate of 3 mm/yr based on fault geometries and slip histories from the Northern Foothills thrust belt, which after comparison to the geodetic rate of ~4 mm/yr, leaves 1 mm/yr of unaccounted-for shortening (Fig. 15). These convergence calculations are based on 10⁴ yr and 10¹ yr data inputs, respectively. Nevertheless, our inference of minimum shortening and almost pure vertical extrusion between the Hines Creek and Denali faults in our region of study aligns with these constraints given our broad 10⁶ regional exhumation rate calculations (0.6–0.9 mm/yr)

for the Between the Hines Creek and Denali faults block (this study; Benowitz et al., 2011a, 2014). The pattern of north-to-south younging in cooling ages for the ⁴⁰Ar/³⁹Ar muscovite, biotite, K-FAT, and AFT and AHe systems toward the north side of the Denali fault is best explained by 18° south-side-up tilting of the Between the Hines Creek and Denali faults block as southern Alaska migrates to the northwest (Fig. 16) (Benowitz et al., 2011a).

Why the Between the Hines Creek and Denali faults block is experiencing a greater rate of vertical extrusion east of ca. 148° W is not clear. The trace of the Hines Creek fault becomes less of a prominent geomorphic feature around 148.0° W, and topography drops off in the Between the Hines Creek and Denali faults block to elevations not high enough to sustain valley glaciers (Fig. 1). The width of the Northern Foothills thrust belt increases to the west of the apex of the Mount Hayes restraining bend at ~147.2° W; hence, deformation may be accommodated across a wider zone (Vallage et al., 2014), but the expansion of the mountain front is not in full alignment with east-to-west cooling age patterns in the Between the Hines Creek and Denali faults block. Longitude 147.2° W is also approximately where the Hines Creek and Denali faults become strike-parallel and near where the last high peak of the Hayes Range lies (Mount Deborah: 3761 m). It is possible that since ca. 6 Ma there has also been a lag in a clear geomorphic response to the broadening of the deformation front to the Nenana Glacier area (Fig. 9). Hence, we leave why deformation drops off to the west of the Nenana Glacier area unresolved but propose that the Between

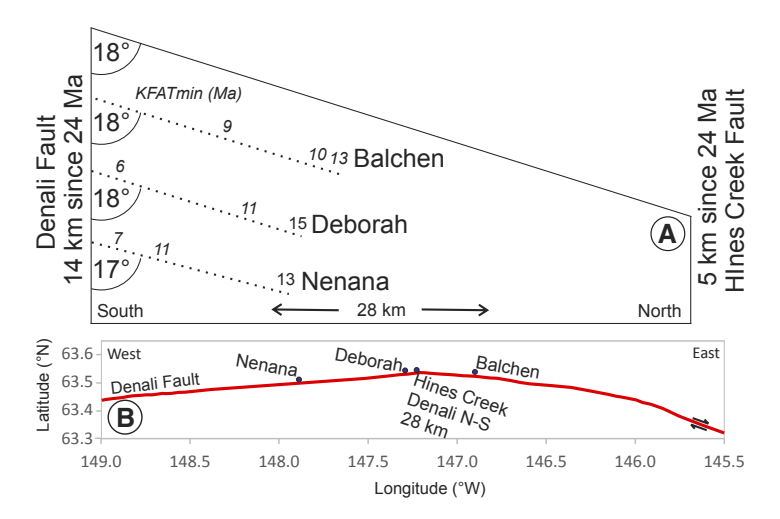


Figure 16. (A) KFAT_{min} cooling ages and inferred tilted isochrons (Benowitz et al., 2011a) and differential depth of exhumation since ca. 24 Ma between the Hines Creek (5 km) and Denali faults (14 km) reflect differential erosion, the Between the Hines Creek and Denali faults block riding up onto the Denali fault, and 18° of south-side-up tilting toward the Denali fault. (B) Locations (longitude) along the Denali fault for the Nenana, Deborah, and Balchen S-N cooling age transects (Fig. 7) and the depth of exhumation comparison between the Denali and Hines Creek faults.

the Hines Creek and Denali faults block is experiencing persistent and locally rapid vertical extrusion because of its fixed geometric position between the Hines Creek and Denali lithospheric-scale faults.

Vertical Extrusion between the Fairweather Transform Fault and the Border Ranges Fault?

How oblique convergence along the Fairweather Transform fault of southeastern Alaska was accommodated and resulted in the formation of the Fairweather Range and its deep exhumation is an open ended question. This region of significant topography is located on the convex side of a restraining bend (McAleer et al., 2009; Lease et al., 2021) to the east of the Fairweather fault and west of the Border Ranges fault, which is a Mesozoic forearc-accretionary complex boundary that reactivated as a Late Cretaceous-Eocene, dextral strike-slip fault (Fig. 17) (Roeske et al., 2003; Pavlis and Roeske, 2007). Glaciated topography between the faults reaches heights of 4671 m at Mount Fairweather. However, to the west of the bend, topography is subdued, only reaching heights of 1684 m at Mount Reaburn. The limited published K-Ar mica ages (closure temperature of ca. 400 °C to 350 °C) are as young as 16.6 ± 0.2 Ma (muscovite) and 7.1 ± 0.2 Ma (biotite) from samples collected east of the Fairweather fault on the outside of the restraining bend, which indicates that this is a region of deep Neogene exhumation. Zircon fission-track cooling ages (closure temperature of ca. 250 °C) west of the Fairweather fault are 27.5 ± 0.5 Ma and 18.8 ± 1.2 Ma, which indicates significantly less Neogene exhumation on the inside of the bend. Rheology inferences indicate that the Yakutat oceanic crust west of the Fairweather Transform is weaker than the neighboring continental crust due to thermal weakening (Brothers et al., 2020), which discounts a strength contrast justification for persistent deeper exhumation in the stronger Fairweather Range throughout the Neogene.

McAleer et al. (2009) acknowledged that the Border Ranges and Fairweather faults acting in tandem could explain the topography and exhumation patterns. The hypothesis was discounted because McAleer et al. (2009) assumed that the Border Ranges fault is a "dead" structure. Yet, that inference may need revision because the fault is locally seismically active (Fig. 17; Doser and Lomas, 2000; Doser and Rodriguez, 2011). McAleer et al. (2009) also presented young AHe cooling ages on both sides of the structure as evidence that the Border Range fault has not accommodated significant vertical displacement. Perhaps invariable across-fault cooling ages, like on the Hines Creek fault, are emblematic of reactivated "backstop" suture zone faults acting as a free face for vertical extrusion, where deformation is distributed across the structure as the uplifted block is tilted on the frontal structure and reverse faults are reactivated and/or develop in the foreland (Bemis et al., 2015; this study). McAleer et al. (2009) and Lease et al. (2021) suggest that a transpressive environ is responsible for the persistent long-term exhumation and topographic development of the Fairweather Range east of the bend (Fig. 17). We concur with this assessment, with the Fairweather Transform and the Border Ranges

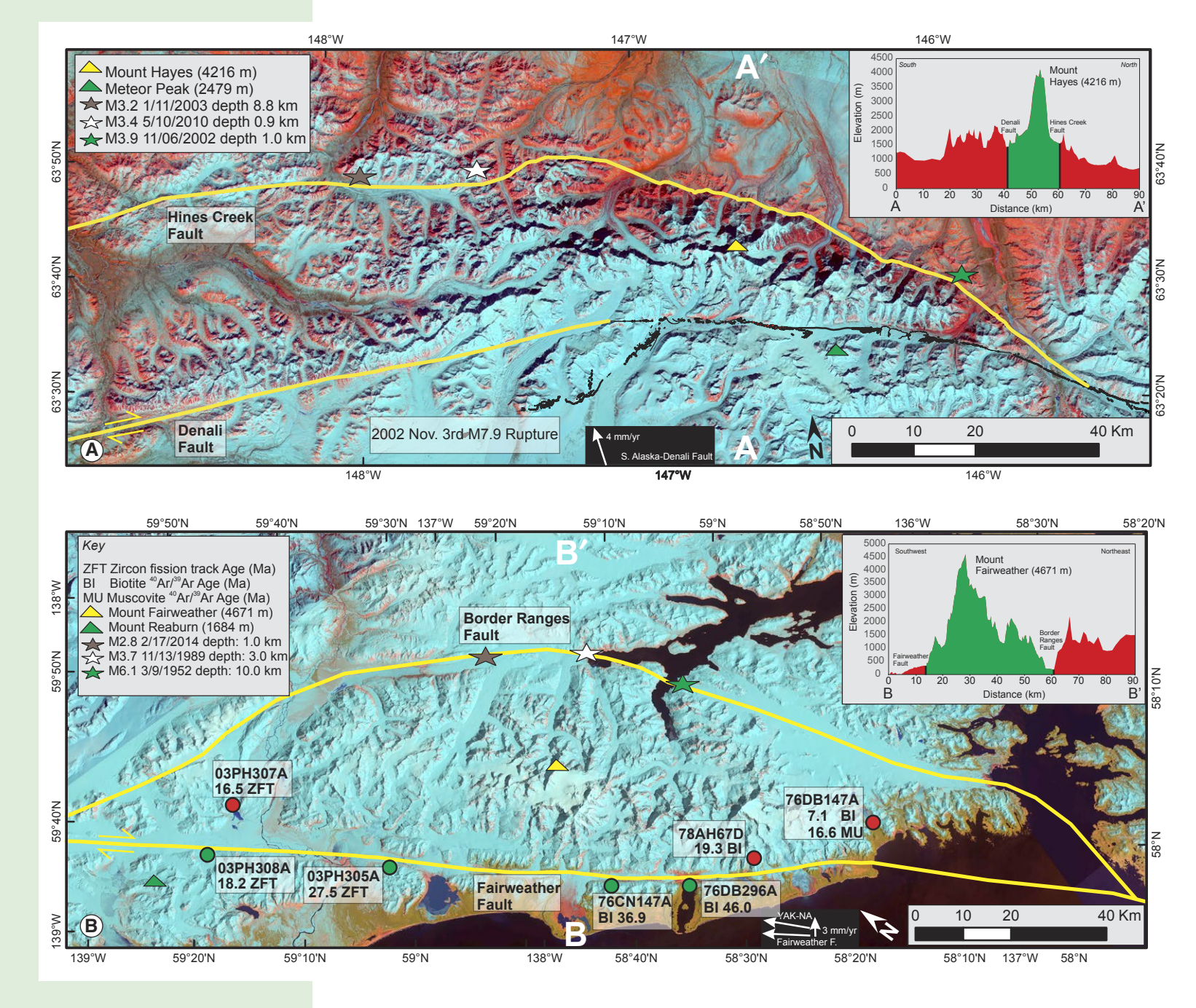


Figure 17. Landsat images show (A) the Between the Hines Creek and Denali faults block and (B) Fairweather Range. Currently available zircon fission track and 40Ar/39Ar mica thermochronological data and sample locations are annotated on the Fairweather Range figure (McAleer et al., 2009; Wilson et al., 2015). Across fault convergence constraints for the Fairweather fault are from McAleer et al. (2009). Across fault convergence constraints for the Denali fault are from Elliott and Freymueller (2020). Selected earthquakes are shown to demonstrate seismic activity on the Hines Creek and Border Ranges fault systems. Inset topographic profiles show topographic breaks across the Denali and Hines Creek faults (A and A') and the Fairweather and Border Ranges faults (B and B'). Fairweather fault (F.) details are in Table S1, see text footnote 1. YAK-NA - Yakutat microplate-North America.

fault acting as free faces to allow rapid vertical extrusion of the Fairweather Range block during transpression.

The Fairweather fault, at least where exposed, is generally very narrow and measured at less than 100 m wide at one site (Witter et al., 2021), similar to the localized and narrow Denali fault. The Alpine fault of New Zealand in places is similarly a narrow and localized fault and has been since at least the Neogene and likely longer (<20 m wide; Kupfer, 1964; Barth et al., 2013). This transpressive fault system has experienced vertical extrusion of crustal blocks between parallel sub-vertical faults (Klepeis et al., 2019). Hence, vertical extrusion of crustal blocks along strike-slip faults is likely a common geodynamic occurrence.

CONCLUSION

By integrating existing and new U-Pb zircon (hornblende, muscovite, biotite and K-feldspar), ⁴⁰Ar/²⁹Ar, AFT, and AHe data, we gained a better understanding of the tectono-magmatic history of the Mount Hayes restraining bend and the high peak region of the Hayes Range. Major findings are:

- (1) The 13° Mount Hayes restraining bend has had a stable long-wavelength geometry since ca. 45 Ma.
- (2) The Denali fault has been a localized structure since ca. 45 Ma with a single strand fault trace width of less than 160 m along the Mount Hayes restraining bend.
- (3) The region of the near Denali fault-focused rapid exhumation in the high peak region of the Hayes Range broadened to the west at ca. 6 Ma and is related to a change in the convergence angle of the Pacific/Yakutat plates to North America.
- (4) The Between the Hines Creek and Denali faults block is riding up and tilting, south side up, against the oblique but primarily dextral-slip Denali fault, which results in younger cooling ages near the fault zone and older cooling ages to the north.
- (5) The Hines Creek fault is an unappreciated structure in the development of topography in the Alaska Range and should be considered in seismic hazard assessments (Fig. 17).
- (6) Late Cretaceous to present arc magmatism is localized in the Alaska Range suture zone far inboard from the subduction zone margin. Upper plate crustal heterogeneities controlling slab dip and lithospheric scale structures acting as magma conduits are likely responsible for this inboard magmatism that continues to the present.

Furthermore, large-scale vertical block extrusion along the free face of parallel faults is responsible for rapid exhumation and the high topography of the Hayes Range, and this is likely a common geodynamic process along strike-slip fault systems. Additionally, long term fault localization and narrow fault zones is a common feature of strike-slip faults with a component of compression. We infer that compression localizes slip onto a single master strand, and the beveling-off of crustal material due to high vertical tectonics rates leads to a narrow fault zone as the development of brittle subsidiary faults is limited through erosion.

The Denali fault (this study), Fairweather fault (McAleer et al., 2009; Witter et al., 2021), and Alpine fault (<20 m wide; Barth et al., 2013) are classic examples.

ACKNOWLEDGMENTS

This research was partially supported by the National Science Foundation (EAR 1828023 and 1550123 to J.A. Benowitz; EAR 1828737 to S. Roeske). The manuscript was improved greatly through detailed reviews by Maurice "Mo" Colpron, Don Murphy, Jim Spotila, and Laura Webb.

REFERENCES CITED

- Allam, A.A., Schulte-Pelkum, V., Ben-Zion, Y., Tape, C., Ruppert, N., and Ross, Z.E., 2017, Ten kilometer vertical Moho offset and shallow velocity contrast along the Denali Fault zone from double-difference tomography, receiver functions, and fault zone head waves: Tectonophysics, v. 721. p. 56-69. https://doi.org/10.1016/i.tecto.2017.09.003.
- Allen, W.K., Ridgway, K.D., Benowitz, J.A., Waldien, T.S., Roeske, S.M., Fitzgerald, P.G., and Gillis, R.J., 2022, Neogene sedimentary record of the evolution of translated strike-slip basin along the Denali fault system: Implications for timing of displacement, composite basin development, and regional tectonics of southern Alaska: Geosphere, v. 18, p. 585–615, https://doi.org/10.1130/GES02435.1.
- Alvarado, A., Audin, L., Nocquet, J.M., Jaillard, E., Mothes, P., Jarrín, P., Segovia, M., Rolandone, F., and Cisneros, D., 2016, Partitioning of oblique convergence in the Northern Andes subduction zone: Migration history and the present-day boundary of the North Andean Sliver in Ecuador: Tectonics, v. 35, p. 1048–1065, https://doi.org/10.1002/2016TC004117.
- Andronikov, A.V., and Mukasa, S.B., 2010, ⁴⁰Ar/⁸⁹Ar eruption ages and geochemical characteristics of Late Tertiary to Quaternary intraplate and arc-related lavas in interior Alaska: Lithos, v. 115, p. 1–14, https://doi.org/10.1016/j.lithos.2009.11.002.
- Athey, J.E., Newberry, R.J., Werdon, M.B., Freeman, L.K., Smith, R.L., and Szumigala, D.J., 2006, Bedrock geologic map of the Liberty Bell area, Fairbanks A-4 Quadrangle, Bonnifield mining district, Alaska: Alaska Division of Geological & Geophysical Surveys Report of Investigation 2006-2, v. 1.0.1, scale 1:50,000, 1 sheet, 98 p. text, https://doi.org/10.14509/15026.
- Bailey, W.R., Holdsworth, R.E., and Swarbrick, R.E., 2000, Kinematic history of a reactivated oceanic suture: The Mamonia Complex Suture Zone, SW Cyprus: Journal of the Geological Society, v. 157, no. 6, p. 1107–1126, https://doi.org/10.1144/jgs.157.6.1107.
- Barth, N.C., Boulton, C., Carpenter, B.M., Batt, G.E., and Toy, V.G., 2013, Slip localization on the southern Alpine fault, New Zealand: Tectonics, v. 32, p. 620–640, https://doi.org/10.1002/tect 20041
- Bauer, M.A., Pavlis, G.L., and Landes, M., 2014, Subduction geometry of the Yakutat terrane, southeastern Alaska: Geosphere, v. 10, p. 1161–1176, https://doi.org/10.1130/GES00852.1.
- Bemis, S.P., and Wallace, W.K., 2007, Neotectonic framework of the north-central Alaska Range foothills, in Ridgway, K.D., et al., eds., Tectonic Growth of a Collisional Continental Margin: Crustal Evolution of Southern Alaska: Geological Society of America Special Paper 431, p. 549–572, https://doi.org/10.1130/20072431(21).
- Bemis, S.P., Carver, G.A., and Koehler, R.D., 2012, The Quaternary thrust system of the northern Alaska Range: Geosphere, v. 8, p. 196–205, https://doi.org/10.1130/GES00695.1.
- Bemis, S.P., Weldon, R.J., and Carver, G.A., 2015, Slip partitioning along a continuously curved fault: Quaternary geologic controls on Denali Fault system slip partitioning, growth of the Alaska Range, and the tectonics of south-central Alaska: Lithosphere, v. 7, no. 3, p. 235–246, https://doi.org/10.1130/L352.1.
- Benowitz, J.A., Layer, P.W., Armstrong, P., Perry, S.E., Haeussler, P.J., Fitzgerald, P.G., and Van-Laningham, S., 2011a, Spatial variations in focused exhumation along a continental-scale strike-slip fault: The Denali Fault of the eastern Alaska Range: Geosphere, v. 7, p. 455–467, https://doi.org/10.1130/GES00589.1.
- Benowitz, J.A., Layer, P.W., and Freeman, L.K., 2011b, ⁴⁰Ar/⁵⁸Ar ages from the East Bonnifield Geologic Map Area, Fairbanks A-1, Fairbanks A-2, Healy D-1, and Healy D-2 Quadrangles, Alaska: Alaska Division of Geological & Geophysical Surveys Raw Data File 2011-2 v. 1.1, 22 p., https://doi.org/10.14509/22482.
- Benowitz, J.A., Haeussler, P.J., Layer, P.W., O'Sullivan, P.B., Wallace, W.K., and Gillis, R.J., 2012, Cenozoic tectono-thermal history of the Tordrillo Mountains, Alaska: Paleocene–Eocene

- ridge subduction, decreasing relief, and late Neogene faulting: Geochemistry, Geophysics, Geosystems, v. 13, https://doi.org/10.1029/2011GC003951.
- Benowitz, J.A., Layer, P.W., and Vanlaningham, S., 2014, Persistent long-term (c. 24 Ma) exhumation in the Eastern Alaska Range constrained by stacked thermochronology, in Jourdan, F., et al., eds., Advances in 40Ar/30Ar Dating: From Archaeology to Planetary Sciences: Geological Society, London, Special Publication 378, p. 225–243, https://doi.org/10.1144/SP378.12.
- Benowitz, J.A., Davis, K., and Roeske, S., 2019, A river runs through it both ways across time: ⁴⁰Ar/⁵⁹Ar detrital and bedrock muscovite geochronology constraints on the Neogene paleodrainage history of the Nenana River system, Alaska Range: Geosphere, v. 15, p. 682– 701, https://doi.org/10.1130/GES01673.1.
- Benowitz, J.A., Michele, L., Cooke, M.L., Terhune, P.J., Herreid, S., Bemis, S.P., Toeneboehn, K., Waldien, T.S., and O'Sullivan, P.B., 2021, Why is Denali (6,194 m) so big?: Caught inside the tectonic wake of a migrating restraining bend: Terra Nova, https://doi.org/10.1111/ter.12571.
- Berkelhammer, S.E., Brueseke, M.E., Benowitz, J.A., Trop, J.M., Davis, K., Layer, P.W., and Weber, M., 2019, Geochemical and geochronological records of tectonic changes along a flat-slab arc-transform junction: Circa 30 Ma to ca. 19 Ma Sonya Creek volcanic field, Wrangell Arc, Alaska: Geosphere, v. 15, p. 1508–1538, https://doi.org/10.1130/GES02114.1.
- Box, S.E., Karl, S.M., Jones, J.V., III, Bradley, D.C., Haeussler, P.J., and O'Sullivan, P.B., 2019, Detrital zircon geochronology along a structural transect across the Kahiltna assemblage in the western Alaska Range: Implications for emplacement of the Alexander–Wrangellia– Peninsular terrane against North America: Geosphere, v. 15, p. 1774–1808, https://doi.org /10.1130/GES02060.1.
- Braun, J., Van der Beek, P., and Batt, G., 2006, Quantitative thermochronology: Numerical methods for the interpretation of thermochronological data: Cambridge University Press, Cambridge, UK, 258 p., https://doi.org/10.1017/CBO9780511616433.
- Brennan, P.R., Gilbert, H., and Ridgway, K.D., 2011, Crustal structure across the central Alaska Range: Anatomy of a Mesozoic collisional zone: Geochemistry, Geophysics, Geosystems, v. 12, https://doi.org/10.1029/2011GC003519.
- Brewer, W.M., and Craddock, C., 1989, Geologic map of the Mount Deborah area, central Alaska Range, Alaska: Alaska Division of Geological & Geophysical Surveys Report of Investigation 89–1, scale 1:63,360, 4 sheets, https://doi.org/10.14509/2467.
- Brothers, D.S., Miller, N.C., Barrie, J.V., Haeussler, P.J., Greene, H.G., Andrews, B.D., Zielke, O., Watt, J., and Dartnell, P., 2020, Plate boundary localization, slip-rates and rupture segmentation of the Queen Charlotte Fault based on submarine tectonic geomorphology: Earth and Planetary Science Letters, v. 530, no. 115882, https://doi.org/10.1016/j.epsl.2019.115882.
- Brueseke, M., Benowitz, J., and Miggins, D., 2021, Newly recognized monogenic volcanism in South-Central Alaska (U.S.A.): The Maclaren River Volcanic Field and implications for the architecture of the subducting Yakutat Slab: Geological Society of America Abstracts with Programs, v. 53, no. 6, https://doi.org/10.1130/abs/2021AM-365640.
- Brueseke, M.E., Benowitz, J.A., Trop, J.M., Davis, K.N., Berkelhammer, S.E., Layer, P.W., and Morter, B.K., 2019, The Alaska Wrangell Arc: ~30 m.y. of subduction-related magmatism along a still active arc-transform junction: Terra Nova, v. 31, p. 59–66, https://doi.org/10.1111/ter.12369.
- Burkett, C.A., Bemis, S.P., and Benowitz, J.A., 2016, Along-fault migration of the Mount McKinley restraining bend of the Denali Fault defined by late Quaternary fault patterns and seismicity, Denali National Park & Preserve, Alaska: Tectonophysics, v. 693, p. 489–506, https://doi.org/10.1016/j.tecto.2016.05.009.
- Caine, J.S., Israel, S.A., Benowitz, J.A., and Murphy, D.A., 2015, A fault rock record of late Eocene strain partitioning along the Denali Fault Zone in Southwestern Yukon: Geological Society of America Abstracts with Programs, v. 47, no. 4, p. 51.
- Caine, J.S., Benzel, W.M., and Benowitz, J.A., 2018, Fault rock evolution, preliminary geochronology, and the record of ductile to brittle, late Eocene–late Miocene strain partitioning along the Denali Fault Zone in Southwestern Yukon, Canada: Cordilleran Tectonics Workshop, Whitehorse, Yukon, Abstracts with Program, p. 19.
- Cole, R.B., Nelson, S.W., Layer, P.W., and Oswald, P.J., 2006, Eocene volcanism above a depleted mantle slab window in southern Alaska: Geological Society of America Bulletin, v. 118, p. 140– 158, https://doi.org/10.1130/B25658.1.
- Csejtey, B., Jr., Mullen, M.W., Cox, D.P., and Stricker, G.D., 1992, Geology and geochronology of the Healy Quadrangle, south-central Alaska: U.S. Geological Survey Miscellaneous Investigations Series Map 1961, scale 1:250,000, 2 sheets, 63 p. text.
- Dewey, J.F., 1977, Suture zone complexities: A review: Tectonophysics, v. 40, no. 1–2, p. 53–67, https://doi.org/10.1016/0040-1951(77)90029-4.

- Dodson, M.H., 1973, Closure temperature in cooling geochronological and petrological systems: Contributions to Mineralogy and Petrology, v. 40, p. 259–274, https://doi.org/10.1007/BF00373790.
- Donelick, R.A., O'Sullivan, P.B., and Ketcham, R.A., 2005, Apatite fission-track analysis: Reviews in Mineralogy and Geochemistry, v. 58, p. 49–94, https://doi.org/10.2138/rmg.2005.58.3.
- Doser, D.I., and Lomas, R., 2000, The transition from strike-slip to oblique subduction in south-eastern Alaska from seismological studies: Tectonophysics, v. 316, p. 45–65, https://doi.org/10.1016/S0040-1951(99)00254-1.
- Doser, D.I., and Rodriguez, H., 2011, A seismotectonic study of the Southeastern Alaska Region: Tectonophysics, v. 497, p. 105–113, https://doi.org/10.1016/j.tecto.2010.10.019.
- Doubrovine, P.V., and Tarduno, J.A., 2008, A revised kinematic model for the relative motion between Pacific oceanic plates and North America since the Late Cretaceous: Journal of Geophysical Research: Solid Earth, v. 113, p. 1–20.
- Dumoulin, J.A., Jones, J.V., III, Box, S.E., Bradley, D.C., Ayuso, R.A., and O'Sullivan, P., 2018, The Mystic subterrane (partly) demystified: New data from the Farewell terrane and adjacent rocks, interior Alaska: Geosphere, v. 14, p. 1501–1543, https://doi.org/10.1130/GES01588.1.
- Dusel-Bacon, C., Day, W.C., and Aleinikoff, J.N., 2013, Geochemistry, petrography, and zircon U-Pb geochronology of Paleozoic metaigneous rocks in the Mount Veta area of east-central Alaska: Implications for the evolution of the westernmost part of the Yukon-Tanana terrane: Canadian Journal of Earth Sciences, v. 50, no. 8, p. 826–846, https://doi.org/10.1139/cjes-2013-0004.
- Dusel-Bacon, C., Holm-Denoma, C.S., Jones, J.V., Aleinikoff, J.N., and Mortensen, J.K., 2017, Detrital zircon geochronology of quartzose metasedimentary rocks from parautochthonous North America, east-central Alaska: Lithosphere, v. 9, p. 927–952, https://doi.org/10.1130/L672.1.
- Eberhart-Phillips, D., Haeussler, P.J., Freymueller, J.T., Frankel, A.D., Rubin, C.M., Craw, P., Ratch-kovski, N.A., Anderson, G., Carver, G.A., Crone, A.J., and Dawson, T.E., 2003, The 2002 Denali Fault earthquake, Alaska: A large magnitude, slip-partitioned event: Science, v. 300, no. 5622, p. 1113–1118, https://doi.org/10.1126/science.1082703.
- Eberhart-Phillips, D., Christensen, D.H., Brocher, T.M., Hansen, R., Ruppert, N.A., Haeussler, P.J., and Abers, G.A., 2006, Imaging the transition from Aleutian subduction to Yakutat collision in central Alaska, with local earthquakes and active source data: Journal of Geophysical Research: Solid Earth, v. 111, p. 1–31.
- Elliott, J., and Freymueller, J.T., 2020, A block model of present-day kinematics of Alaska and western Canada: Journal of Geophysical Research: Solid Earth, v. 125, no. e2019JB018378, https://doi.org/10.1029/2019JB018378.
- Elliott, J.L., Larsen, C.F., Freymueller, J.T., and Motyka, R.J., 2010, Tectonic block motion and glacial isostatic adjustment in southeast Alaska and adjacent Canada constrained by GPS measurements: Journal of Geophysical Research: Solid Earth, v. 115, https://doi.org/10.1029 //2009JB007139.
- Engebretson, D.C., Cox, A., and Gordon, R.G., 1985, Relative Motions Between Oceanic and Continental Plates in the Pacific Basin: Geological Society of America Special Paper 206, 59 p., https://doi.org/10.1130/SPE206-p1.
- Estève, C., Audet, P., Schaeffer, A.J., Schutt, D.L., Aster, R.C., and Cubley, J.F., 2020, Seismic evidence for craton chiseling and displacement of lithospheric mantle by the Tintina fault in the northern Canadian Cordillera: Geology, v. 48, p. 1120–1125, https://doi.org/10.1130/G47688.1.
- Farley, K.A., 2002, (U-Th)/He dating: Techniques, calibrations, and applications: Reviews in Mineralogy and Geochemistry, v. 47, p. 819–844, https://doi.org/10.2138/rmg.2002.47.18.
- Farley, K.A., Wolf, R.A., and Silver, L.T., 1996, The effects of long alpha-stopping distances on (U-Th)/He ages: Geochimica et Cosmochimica Acta, v. 60, p. 4223–4229, https://doi.org/10.1016/S0016-7037(96)00193-7, https://doi.org/10.1016/S0016-7037(96)00193-7.
- Fattaruso, L.A., Cooke, M.L., and Dorsey, R.J., 2014, Sensitivity of uplift patterns to dip of the San Andreas fault in the Coachella Valley, California: Geosphere, v. 10, p. 1235–1246, https://doi.org/10.1130/GES01050.1.
- Federschmidt, S., 2014, Paleoseismic and structural characterization of the Hines Creek Fault: Denali National Park and Preserve, Alaska [M.S. thesis]: Lexington, Kentucky, USA, University of Kentucky, 102 p.
- Fichtner, A., Saygin, E., Taymaz, T., Cupillard, P., Capdeville, Y., and Trampert, J., 2013, The deep structure of the North Anatolian fault zone: Earth and Planetary Science Letters, v. 373, p. 109– 117, https://doi.org/10.1016/j.epsl.2013.04.027.
- Fitzgerald, P.G., Stump, E., and Redfield, T.F., 1993, Late Cenozoic uplift of Denali and its relation to relative plate motion and fault morphology: Science, v. 259, p. 497–499, https://doi.org/10 .1126/science.259.5094.497.

- Fitzgerald, P.G., Baldwin, S.L., Webb, L.E., and O'Sullivan, P.B., 2006, Interpretation of (U-Th)/He single grain ages from slowly cooled crustal terranes: A case study from the Transantarctic Mountains of southern Victoria Land: Chemical Geology, v. 225, no. 1–2, p. 91–120, https://doi.org/10.1016/j.chemgeo.2005.09.001.
- Fitzgerald, P.G., Roeske, S.M., Benowitz, J.A., Riccio, S.J., Perry, S.E., and Armstrong, P.A., 2014, Alternating asymmetric topography of the Alaska range along the strike-slip Denali Fault: Strain partitioning and lithospheric control across a terrane suture zone: Tectonics, v. 33, p. 1519–1533, https://doi.org/10.1002/2013TC003432.
- Fitzgerald, P.G., Warfel, T.S., Benowitz, J., Ridgway, K., Allen, W., and O'Sullivan, P.B., 2018, Exhumation along the southern side of the eastern Denali Fault of South-Central Alaska: Evaluating the importance of fault geometry vs terrane rheology: Abstract T53A–02B, presented at 2018 Fall Meeting, American Geophysical Union, Washington, D.C., 10–14 December.
- Flowers, R.M., Ketcham, R.A., Shuster, D.L., and Farley, K.A., 2009, Apatite (U-Th)/He thermochronometry using a radiation damage accumulation and annealing model: Geochimica et Cosmochimica Acta, v. 73, p. 2347–2365, https://doi.org/10.1016/j.gca.2009.01.015.
- Fuis, G.S., Moore, T.E., Plafker, G., Brocher, T.M., Fisher, M.A., Mooney, W.D., Nokleberg, W.J., Page, R.A., Beaudoin, B.C., Christensen, N.I., and Levander, A.R., 2008, Trans-Alaska Crustal Transect and continental evolution involving subduction underplating and synchronous foreland thrusting: Geology, v. 36, p. 267–270, https://doi.org/10.1130/G24257A.1.
- Gansser, A., 1980, The significance of the Himalayan suture zone: Tectonophysics, v. 62, p. 37–52, https://doi.org/10.1016/0040-1951(80)90134-1.
- Garver, J.I., and Davidson, C.M., 2015, Southwestern Laurentian zircons in Upper Cretaceous flysch of the Chugach-Prince William terrane in Alaska: American Journal of Science, v. 315, p. 537–556, https://doi.org/10.2475/06.2015.02.
- Gehrels, G., and Pecha, M., 2014, Detrital zircon U-Pb geochronology and Hf isotope geochemistry of Paleozoic and Triassic passive margin strata of western North America: Geosphere, v. 10, p. 49–65, https://doi.org/10.1130/GES00889.1.
- Gehrels, G., Valencia, V., and Pullen, A., 2006, Detrital zircon geochronology by laser-ablation multicollector ICPMS at the Arizona LaserChron Center: The Paleontological Society Papers, 12, p. 67–76. https://doi.org/10.1017/S1089332600001352.
- Gehrels, G.E., Valencia, V.A., and Ruiz, J., 2008, Enhanced precision, accuracy, efficiency, and spatial resolution of U-Pb ages by laser ablation-multicollector-inductively coupled plasma-mass spectrometry: Geochemistry, Geophysics, Geosystems, v. 9, Q03017, https://doi.org/10.1029 /2007GC001805.
- Gómez-Vasconcelos, M.G., Luis Macías, J., Avellán, D.R., Sosa-Ceballos, G., Garduño-Monroy, V.H., Cisneros-Máximo, G., Layer, P.W., Benowitz, J., López-Loera, H., López, F.M., and Perton, M., 2020, The control of preexisting faults on the distribution, morphology, and volume of monogenetic volcanism in the Michoacán-Guanajuato Volcanic Field: Geological Society of America Bulletin, v. 132. p. 2455–2474. https://doi.org/10.1130/B35397.1
- Haeussler, P.J., 2008, An overview of the neotectonics of interior Alaska: Far-field deformation from the Yakutat microplate collision, in Freymueller, J.T., Haeussler, P.J., Wesson, R.L., and Ekström, G., eds., Active Tectonics and Seismic Potential of Alaska: Washington, D.C., American Geophysical Union, Geophysical Monograph Series, v. 179, p. 83–108.
- Haeussler, P.J., 2009, Surface rupture map of the 2002 M 7.9 Denali Fault Earthquake, Alaska: Digital data: U.S. Geological Survey, Digital Data Series, 422, scale 1:500, 1 sheet, 13 p. text.
- Haeussler, P.J., Matmon, A., Schwartz, D.P., and Seitz, G.G., 2017, Neotectonics of interior Alaska and the late Quaternary slip rate along the Denali Fault system: Geosphere, v. 13, p. 1445–1463, https://doi.org/10.1130/GES01447.1.
- Harrison, T.M., Célérier, J., Aikman, A.B., Hermann, J., and Heizler, M.T., 2009, Diffusion of 40Ar in muscovite: Geochimica et Cosmochimica Acta, v. 73, p. 1039–1051, https://doi.org/10.1016/j.gca.2008.09.038.
- Hatem, A.E., Cooke, M.L., and Madden, E.H., 2015, Evolving efficiency of restraining bends within wet kaolin analog experiments: Journal of Geophysical Research: Solid Earth, v. 120, p. 1975– 1992, https://doi.org/10.1002/2014JB011735.
- Herriott, T.M., Crowley, J.L., Schmitz, M.D., Wartes, M.A., and Gillis, R.J., 2019, Exploring the law of detrital zircon: LA-ICP-MS and CA-TIMS geochronology of Jurassic forearc strata, Cook Inlet, Alaska, USA: Geology, v. 47, p. 1044–1048, https://doi.org/10.1130/G46312.1.
- Hillhouse, J.W., and Coe, R.S., 1994, Paleomagnetic data from Alaska, in Plafker, G., and Berg, H.C., eds., The Geology of Alaska: Boulder, Colorado, Geological Society of America, The Geology of North America, v. G-1, p. 797–812.

- Hults, C.P., Wilson, F.H., Donelick, R.A., and O'Sullivan, P.B., 2013, Two flysch belts having distinctly different provenance suggest no stratigraphic link between the Wrangellia composite terrane and the paleo-Alaskan margin: Lithosphere, v. 5, p. 575–594, https://doi.org /10.1130/L310.1.
- Jadamec, M.A., Billen, M.I., and Roeske, S.M., 2013, Three-dimensional numerical models of flat slab subduction and the Denali Fault driving deformation in south-central Alaska: Earth and Planetary Science Letters, v. 376, p. 29–42, https://doi.org/10.1016/j.epsl.2013.06.009.
- Jicha, B.R., Garcia, M.O., and Wessel, P., 2018, Mid-Cenozoic Pacific plate motion change: Implications for the northwest Hawaiian Ridge and circum-Pacific: Geology, v. 46, p. 939–942, https:// doi.org/10.1130/G45175.1.
- Jones, D., Siberling, N., Gilbert, W., and Coney, P., 1982, Character, distribution, and tectonic significance of accretionary terranes in the central Alaska Range: Journal of Geophysical Research: Solid Earth, v. 87, p. 3709–3717, https://doi.org/10.1029/JB087iB05p03709.
- Jones, J., Caine, J., Holm-Denoma, C., Ryan, J., Benowitz, J., and Drenth, B., 2017, Unraveling the boundary between the Yukon-Tanana terrane and the parautochthonous North America in eastern Alaska: Geological Society of America Abstracts with Programs, v. 49, no. 6, https:// doi.org/10.1130/abs/2017AM-304142.
- Jones, J.V., Todd, E., Box, S.E., Haeussler, P.J., Holm-Denoma, C.S., Karl, S.M., Graham, G.E., Bradley, D.C., Kylander-Clark, A.R., Friedman, R.M., and Layer, P.W., 2021, Cretaceous to Oligocene magmatic and tectonic evolution of the western Alaska Range: Insights from U-Pb and ⁴⁰Ar/²⁰Ar geochronology: Geosphere, v. 17, p. 118–153, https://doi.org/10.1130/GES02303.1.
- Keough, B.M., and Ridgway, K.D., 2021, Tectonic growth of the late Paleozoic-middle Mesozoic northwestern margin of Laurentia and implications for the Farewell terrane: Stratigraphic, structural, and provenance records from the Central Alaska Range: Tectonics, v. 40, https://doi.org/10.1029/2021TC006764.
- Ketcham, R.A., 2005, Forward and inverse modeling of low-temperature thermochronometry data: Reviews in Mineralogy and Geochemistry, v. 58, p. 275–314, https://doi.org/10.2138 /rmg.2005.58.11.
- Klepeis, K., Webb, L., Blatchford, H., Schwartz, J., Jongens, R., Turnbull, R., and Stowell, H., 2019, Deep slab collision during Miocene subduction causes uplift along crustal-scale reverse faults in Fiordland, New Zealand: GSA Today, v. 29, p. 4–10, https://doi.org/10.1130/GSATG399A.1.
- Koehler, R.D., Farrell, R.-E., Burns, P.A.C., and Combellick, R.A., 2012, Quaternary faults and folds in Alaska: A digital database: State of Alaska Department of Natural Resources, Division of Geological & Geophysical Surveys Miscellaneous Publication 141, 31 p.
- Koons, P.O., Norris, R.J., Craw, D., and Cooper, A.F., 2003, Influence of exhumation on the structural evolution of transpressional plate boundaries: An example from the Southern Alps, New Zealand: Geology, v. 31, no. 1, p. 3–6, https://doi.org/10.1130/0091-7613(2003)031<0003: IOEOTS>2.0.CO:2.
- Kupfer, D.H., 1964, Width of the Alpine fault zone, New Zealand: New Zealand Journal of Geology and Geophysics, v. 7, no. 4, p. 685–701, https://doi.org/10.1080/00288306.1964.10428125.
- Lara, L.E., Cembrano, J., and Lavenu, A., 2008, Quaternary vertical displacement along the Liquiñe-Ofqui fault zone: Differential uplift and coeval volcanism in the Southern Andes?: International Geology Review, v. 50, p. 975–993, https://doi.org/10.2747/0020-6814.50.11.975.
- Lease, R.O., Haeussler, P.J., and O'Sullivan, P., 2016, Changing exhumation patterns during Cenozoic growth and glaciation of the Alaska Range: Insights from detrital thermochronology and geochronology: Tectonics, v. 35, p. 934–955, https://doi.org/10.1002/2015TC004067.
- Lease, R.O., Haeussler, P.J., Witter, R.C., Stockli, D.F., Bender, A.M., Kelsey, H.M., and O'Sullivan, P.B., 2021, Extreme Quaternary plate boundary exhumation and strike slip localized along the southern Fairweather fault, Alaska, USA: Geology, v. 49, no. 5, p. 602–606, https://doi .org/10.1130/G48464.1.
- Löbens, S., Oriolo, S., Benowitz, J., Wemmer, K., Layer, P., and Siegesmund, S., 2017, Late Paleozoic deformation and exhumation in the Sierras Pampeanas (Argentina): "Ar/" Ar-feldspar dating constraints: International Journal of Earth Sciences, v. 106, p. 1991–2003, https://doi.org/10.1007/s00531-016-1403-3.
- Lovera, O.M., Grove, M., and Harrison, T.M., 2002, Systematic analysis of K-feldspar ⁴⁰Ar/⁵⁸Ar step heating results II: Relevance of laboratory argon diffusion properties to nature: Geochimica et Cosmochimica Acta, v. 66, p. 1237–1255, https://doi.org/10.1016/S0016-7037(01)00846-8.
- Mann, P., 2007, Global catalogue, classification and tectonic origins of restraining- and releasing bends on active and ancient strike-slip fault systems, in Cunningham, W.D., and Mann, P., eds., Tectonics of Strike-Slip Restraining and Releasing Bends: Geological Society, London, Special Publication 290, p. 13–142, https://doi.org/10.1144/SP290.2.

- Manselle, P., Brueseke, M.E., Trop, J.M., Benowitz, J.A., Snyder, D.C., and Hart, W.K., 2020, Geochemical and stratigraphic analysis of the Chisana Formation, Wrangellia terrane, eastern Alaska: Insights into Early Cretaceous magmatism and tectonics along the northern Cordilleran margin: Tectonics, v. 39, no. e2020TC006131, https://doi.org/10.1029 /2020TC006131.
- Mazzotti, S., and Hyndman, R.D., 2002, Yakutat collision and strain transfer across the northern Canadian Cordillera: Geology, v. 30, p. 495–498, https://doi.org/10.1130/0091-7613(2002)030 <0495:YCASTA>2.0.CO:2.
- McAleer, R.J., Spotila, J.A., Enkelmann, E., and Berger, A.L., 2009, Exhumation along the Fairweather fault, southeastern Alaska, based on low-temperature thermochronometry: Tectonics, v. 28, https://doi.org/10.1029/2007TC002240.
- McDermott, R.G., Ault, A.K., Caine, J.S., and Thomson, S.N., 2019, Thermotectonic history of the Kluane Ranges and evolution of the eastern Denali fault zone in southwestern Yukon, Canada: Tectonics, v. 38, p. 2983–3010, https://doi.org/10.1029/2019TC005545.
- McDermott, R.G., Ault, A.K., and Caine, J.S., 2021, Dating fault damage along the eastern Denali fault zone with hematite (U-Th)/He thermochronometry: Earth and Planetary Science Letters, v. 563, no. 116872, https://doi.org/10.1016/j.epsl.2021.116872.
- Miller, M.L., Bradley, D.C., Bundtzen, T.K., and McClelland, W., 2002, Late Cretaceous through Cenozoic strike-slip tectonics of southwestern Alaska: The Journal of Geology, v. 110, p. 247–270, https://doi.org/10.1086/339531.
- Miller, M.S., O'Driscoll, L.J., Porritt, R.W., and Roeske, S.M., 2018, Multiscale crustal architecture of Alaska inferred from P receiver functions: Lithosphere, v. 10, p. 267–278, https://doi.org /10.1130/L701.1.
- Moser, A.C., Evans, J.P., Ault, A.K., Janecke, S.U., and Bradbury, K.K., 2017, (U–Th)/He thermochronometry reveals Pleistocene punctuated deformation and synkinematic hematite mineralization in the Mecca Hills, southernmost San Andreas Fault zone: Earth and Planetary Science Letters, v. 476, p. 87–99, https://doi.org/10.1016/j.epsl.2017.07.039.
- Mueller, M.A., Licht, A., Campbell, C., Ocakoğlu, F., Taylor, M.H., Burch, L., Ugrai, T., Kaya, M., Kurtoğlu, B., Coster, P.M.C., Métais, G., and Beard, K.C., 2019, Collision chronology along the İzmir–Ankara–Erzincan suture zone: Insights from the Sarıcakaya Basin, western Anatolia: Tectonics, v. 38, p. 3652–3674, https://doi.org/10.1029/2019TC005683.
- Niemi, N.A., Buscher, J.T., Spotila, J.A., House, M.A., and Kelley, S.A., 2013, Insights from low-temperature thermochronometry into transpressional deformation and crustal exhumation along the San Andreas fault in the western Transverse Ranges, California: Tectonics, v. 32, p. 1602–1622, https://doi.org/10.1002/2013TC003377.
- Nokleberg, W.J., Jones, D.L., and Silberling, N.J., 1985, Origin and tectonic evolution of the Maclaren and Wrangellia terranes, eastern Alaska Range, Alaska: Geological Society of America Bulletin, v. 96, p. 1251–1270, https://doi.org/10.1130/0016-7606(1985)96<1251:OATEOT>2 0.CO:2.
- Nokleberg, W.J., Aleinikoff, J.N., Dutro, J.T., Jr., Lanphere, M.A., Silberling, N.J., Silva, S.R., Smith, T.E., and Turner, D.L., 1992, Map, tables, and summary of fossil and isotopic age data, Mount Hayes Quadrangle, eastern Alaska Range, Alaska: U.S. Geological Survey Miscellaneous Field Studies Map 1996-D, scale 1:250,000, 1 sheet, 43 p. text.
- Nokleberg, W.J., Aleinikoff, J.N., Bundtzen, T.K., and Hanshaw, M.N., 2013, Geologic strip map along the Hines Creek fault showing evidence for Cenozoic displacement in the western Mount Hayes and northeastern Healy quadrangles, eastern Alaska Range, Alaska: U.S. Geological Survey Scientific Investigations Map 3238, pamphlet 29, scale 1:63,360, 35 p. text, https:// doi.org/10.3133/sim3238.
- Oldow, J.S., Bally, A.W., and Avé Lallemant, H.G., 1990, Transpression, orogenic float, and lithospheric balance: Geology, v. 18, no. 10, p. 991–994, https://doi.org/10.1130/0091-7613(1990)018 <0991:TOFALB>2.3.CO:2.
- Pavlis, T.L., and Roeske, S.M., 2007, The Border Ranges fault system, southern Alaska, in Ridgway, K.D., Trop, J.M., Glen, J.M.G., and O'Neill, J.M., eds., Tectonic Growth of a Collisional Continental Margin: Crustal Evolution of Southern Alaska: Geological Society of America Special Paper 431, p. 95–128, https://doi.org/10.1130/2007.2431(05).
- Perry, S.E., 2014, Thermotectonic evolution of the Alaska Range: Low-temperature thermochronologic constraints [Ph.D. thesis]: Syracuse, New York, Syracuse University, 844 p.
- Personius, S.F., Crone, A.J., Burns, P.A., and Reitman, N.G., 2017, Recurrent Holocene movement on the Susitna Glacier Thrust Fault: The structure that initiated the M w 7.9 Denali Fault earthquake, Central Alaska: Bulletin of the Seismological Society of America, v. 107, p. 1593–1609, https://doi.org/10.1785/0120160286.

- Redfield, T.F., Scholl, D.W., Fitzgerald, P.G., and Beck, M.E., Jr, 2007, Escape tectonics and the extrusion of Alaska: Past, present, and future: Geology, v. 35, p. 1039–1042, https://doi.org/10.1130/G23799A.1.
- Regan, S.P., Benowitz, J.A., and Holland, M.E., 2020, A plutonic brother from another magma mother: Disproving the Eocene Foraker–McGonagall pluton piercing point and implications for long-term slip on the Denali Fault: Terra Nova, v. 32, p. 66–74, https://doi.org/10.1111/ter.12437.
- Regan, S.P., Benowitz, J.A., Waldien, T.S., Holland, M.E., Roeske, S.M., O'Sullivan, P., and Layer, P., 2021, Long distance plutonic relationships demonstrate 33 million years of strain partitioning along the Denali fault: Terra Nova, v. 33, 630–640, https://doi.org/10.1111/ter.12555.
- Reiners, P.W., and Brandon, M.T., 2006, Using thermochronology to understand orogenic erosion:
 Annual Review of Earth and Planetary Sciences, v. 34, p. 419–466, https://doi.org/10.1146/annurev.earth.34.031405.125202.
- Reiners, P.W., and Farley, K.A., 2001, Influence of crystal size on apatite (U-Th)/He thermochronology: An example from the Bighorn Mountains, Wyoming: Earth and Planetary Science Letters, v. 188, p. 413–420, https://doi.org/10.1016/S0012-821X(01)00341-7.
- Reiners, P.W., Ehlers, T.A., and Zeitler, P.K., 2005, Past, present, and future of thermochronology: Reviews in Mineralogy and Geochemistry, v. 58, p. 1–18, https://doi.org/10.2138/rmg.2005.58.1.
- Renne, P.R., Mundil, R., Balco, G., Min, K., and Ludwig, K.R., 2010, Joint determination of ⁴⁰K decay constants and ⁴⁰Ar*/⁴⁰K for the Fish Canyon sanidine standard, and improved accuracy for ⁴⁰Ar/⁵⁹Ar geochronology: Geochimica et Cosmochimica Acta, v. 74, p. 5349–5367, https://doi.org/10.1016/j.gca.2010.06.017.
- Riccio, S.J., Fitzgerald, P.G., Benowitz, J.A., and Roeske, S.M., 2014, The role of thrust faulting in the formation of the eastern Alaska Range: Thermochronological constraints from the Susitna Glacier thrust fault region of the intracontinental strike-slip Denali Fault system: Tectonics, v. 33, p. 2195–2217, https://doi.org/10.1002/2014TC003646.
- Ridgway, K.D., Trop, J.M., Nokleberg, W.J., Davidson, C.M., and Eastham, K.R., 2002, Mesozoic and Cenozoic tectonics of the eastern and central Alaska Range: Progressive basin development and deformation in a suture zone: Geological Society of America Bulletin, v. 114, p. 1480–1504, https://doi.org/10.1130/0016-7606(2002)114<1480:MACTOT>-2.0.CO;2.
- Ridgway, K.D., Thoms, E.E., Layer, P.W., Lesh, M.E., White, J.M., and Smith, S.V., 2007, Neogene transpressional foreland basin development on the north side of the central Alaska Range, Usibelli Group and Nenana Gravel, Tanana basin, in Ridgway, K.D., Trop, J.M., Glen, J.M.G., and O'Neill, J.M., eds., Tectonic Growth of a Collisional Continental Margin: Crustal Evolution of Southern Alaska: Geological Society of America Special Paper 431, p. 507–547, https://doi.org/10.1130/2007.2431(20).
- Roeske, S.M., Snee, L.W., and Pavlis, T.L., 2003, Dextral-slip reactivation of an arc-forearc boundary during Late Cretaceous–Early Eocene oblique convergence in the northern Cordillera, in Sisson, V.B., Roeske, S.M., and Pavlis, T.L., eds., Geology of a Transpressional Orogen Developed during Ridge-Trench Interaction along the North Pacific Margin: Geological Society of America Special Paper 371, p. 141–169, https://doi.ora/10.1130/0-8137-2371-X.141.
- Roeske, S.M., Till, A., Foster, D., and Sample, J., 2007, Introduction, in Roeske, S.M., Till, A.B., Foster, D.A., and Sample, J.C., eds., Exhumation Associated with Continental Strike-Slip Fault Systems: Geological Society of America Special Paper 434, p. vii–x, https://doi.org/10.1130/978-0-8137-2434-8(2007)434[vii:1]2.0.C0;2.
- Roeske, S.M., Benowitz, J.A., Huff, C., Riccio, S., Fitzgerald, P.G., Perry, S.E., and Layer, P.W., 2011, Variable strain partitioning with depth along the dextral Denali Fault in the eastern Alaska Range: Geological Society of America Abstracts with Programs, v. 43, no. 5, p. 128–129.
- Romero, M.C., Ridgway, K.D., and Gehrels, G.E., 2020, Geology, U-Pb geochronology, and Hf isotope geochemistry across the Mesozoic Alaska Range suture zone (south-central Alaska): Implications for Cordilleran collisional processes and tectonic growth of North America: Tectonics. v. 39. https://doi.org/10.1029/2019TC005946.
- Schartman, A., Enkelmann, E., Garver, J.I., and Davidson, C.M., 2019, Uplift and exhumation of the Russell Fiord and Boundary blocks along the northern Fairweather transform fault, Alaska: Lithosphere, v. 11, p. 232–251, https://doi.org/10.1130/L1011.1.
- Sippl, C., 2016, Moho geometry along a north-south passive seismic transect through Central Australia: Tectonophysics, v. 676, p. 56–69, https://doi.org/10.1016/j.tecto.2016.03.031.
- Sone, M., and Metcalfe, I., 2008, Parallel Tethyan sutures in mainland Southeast Asia: New insights for Palaeo-Tethys closure and implications for the Indosinian orogeny: Comptes Rendus Geoscience, v. 340, p. 166–179, https://doi.org/10.1016/j.crte.2007.09.008.
- Spotila, J.A., and Berger, A.L., 2010, Exhumation at orogenic indentor corners under long-term glacial conditions: Example of the St. Elias orogen, Southern Alaska: Tectonophysics, v. 490, p. 241–256, https://doi.org/10.1016/j.tecto.2010.05.015.

- Spotila, J.A., House, M.A., Niemi, N.A., Brady, R.C., Oskin, M., and Buscher, J.T., 2007, Patterns of bedrock uplift along the San Andreas fault and implications for mechanisms of transpression, in Roeske, S.M., Till, A.B., Foster, D.A., and Sample, J.C., eds., Exhumation Associated with Continental Strike-Slip Fault Systems: Geological Society of America Special Paper 434, p. 15–33, https://doi.org/10.1130/2007.2434(02).
- Sylvester, A.G., 1988, Strike-slip faults: Geological Society of America Bulletin, v. 100, p. 1666–1703, https://doi.org/10.1130/0016-7606(1988)100<1666:SSF>2.3.CO;2.
- Tagami, T., and O'Sullivan, P.B., 2005, Fundamentals of fission-track thermochronology: Reviews in Mineralogy and Geochemistry, v. 58, p. 19–47, https://doi.org/10.2138/rmg.2005.58.2.
- Tait, L.D., 2017, Strain and vorticity analysis of mid-crustal rocks exhumed along the Denali Fault in the Eastern Alaska Range [M.S. thesis]: Davis, California, University of California, 76 p.
- Terhune, P.J., Benowitz, J.A., Trop, J.M., O'Sullivan, P.B., Gillis, R.J., and Freymueller, J.T., 2019, Cenozoic tectono-thermal history of the southern Talkeetna Mountains, Alaska: Insights into a potentially alternating convergent and transform plate margin: Geosphere, v. 15, p. 1539–1576, https://doi.org/10.1130/GES02008.1
- Thrupp, G.A., and Coe, R.S., 1986, Early Tertiary paleomagnetic evidence and the displacement of southern Alaska: Geology, v. 14, p. 213–217, https://doi.org/10.1130/0091-7613(1986)14<213: ETPEAT>2.0.CO;2.
- Trop, J.M., and Ridgway, K.D., 2007, Mesozoic and Cenozoic tectonic growth of southern Alaska: A sedimentary basin perspective, in Ridgway, K.D., Trop, J.M., Glen, J.M.G., and O'Neill, J.M., eds., Tectonic Growth of a Collisional Continental Margin: Crustal Evolution of Southern Alaska: Geological Society of America Special Paper 431, p. 55–94, https://doi.org/10.1130/2007.2431(04).
- Trop, J.M., Benowitz, J., Cole, R.B., and O'Sullivan, P., 2019, Cretaceous to Miocene magmatism, sedimentation, and exhumation within the Alaska Range suture zone: A polyphase reactivated terrane boundary: Geosphere, v. 15, p. 1066–1101, https://doi.org/10.1130/GES02014.1.
- Trop, J.M., Benowitz, J.A., Koepp, D.Q., Sunderlin, D., Brueseke, M.E., Layer, P.W., and Fitzgerald, P.G., 2020, Stitch in the ditch: Nutzotin Mountains (Alaska) fluvial strata and a dike record ca. 117–114 Ma accretion of Wrangellia with western North America and initiation of the Totschunda fault: Geosphere, v. 16, p. 82–110, https://doi.org/10.1130/GES02127.1.
- Trop, J.M., Benowitz, J.A., Kirby, C.S., and Brueseke, M.E., 2022, Geochronology of the Wrangell Arc: Spatial-temporal evolution of slab edge magmatism along a flat slab subduction-transform transition, Alaska-Yukon: Geosphere, v. 18, p. 19–48, https://doi.org/10.1130/GES02417.1.
- Vallage, A., Deves, M.H., Klinger, Y., King, G.C. and Ruppert, N.A., 2014, Localized slip and distributed deformation in oblique settings: The example of the Denali fault system, Alaska: Geophysical Journal International, v. 197, p. 1284–1298, https://doi.org/10.1093/gji/ggu100.

- Veenstra, E., Christensen, D.H., Abers, G.A., and Ferris, A., 2006, Crustal thickness variation in south-central Alaska: Geology, v. 34, p. 781–784, https://doi.org/10.1130/G22615.1.
- Wahrhaftig, C., Turner, D.L., Weber, F.R., and Smith, T.E., 1975, Nature and timing of movement on Hines Creek strand of Denali Fault system, Alaska: Geology, v. 3, p. 463–466, https://doi .org/10.1130/0091-7613(1975)3<463:NATOMO>2.0.CO:2.
- Waldien, T.S., Roeske, S.M., Benowitz, J.A., Allen, W.K., Ridgway, K.D., and O'Sullivan, P.B., 2018, Late Miocene to Quaternary evolution of the McCallum Creek thrust system, Alaska: Insights for range-boundary thrusts in transpressional orogens: Geosphere, v. 14, p. 2379–2406, https:// doi.org/10.1130/GES01676.1.
- Waldien, T.S., Roeske, S.M., and Benowitz, J.A., 2021a, Tectonic underplating and dismemberment of the Maclaren-Kluane schist records Late Cretaceous terrane accretion polarity and ~480 km of Post-52 Ma dextral displacement on the Denali Fault: Tectonics, v. 40, no. e2020TC006677, https://doi.org/10.1029/2020TC006677.
- Waldien, T.S., Roeske, S.M., Benowitz, J.A., Twelker, E., and Miller, M.S., 2021b, Oligocene–Neogene lithospheric-scale reactivation of Mesozoic terrane accretionary structures in the Alaska Range suture zone, southern Alaska, USA: Geological Society of America Bulletin, v. 133, p. 691–716, https://doi.org/10.1130/B35665.1.
- Waldien, T.S., Lease, R.O., Roeske, S.M., Benowitz, J.A., and O'Sullivan, P.B., 2022, The role of preexisting upper plate strike-slip faults during long-lived (ca. 30 Myr) oblique flat slab subduction, southern Alaska: Earth and Planetary Science Letters, v. 577, no. 117242, https://doi .org/10.1016/j.epsl.2021.117242.
- Wech, A.G., 2016, Extending Alaska's plate boundary: Tectonic tremor generated by Yakutat subduction: Geology, v. 44, p. 587–590, https://doi.org/10.1130/G37817.1.
- Westerweel, J., Licht, A., Cogné, N., Roperch, P., Dupont-Nivet, G., Kay Thi, M., Swe, H.H., Huang, H., Win, Z., and Wa Aung, D., 2020, Burma terrane collision and northward indentation in the Eastern Himalayas recorded in the Eocene–Miocene Chindwin Basin (Myanmar): Tectonics, v. 39, no. e2020TC006413, https://doi.org/10.1029/2020TC006413.
- Wilson, F.H., Hults, C.P., Mull, C.G., and Karl, S.M., 2015, Geologic Map of Alaska: U.S. Geological Survey Scientific Investigations Map 3340, scale 1:1,584,000, 2 sheets, 197 p. text.
- Witter, R.C., Bender, A.M., Scharer, K.M., DuRoss, C.B., Haeussler, P.J., and Lease, R.O., 2021, Geomorphic expression and slip rate of the Fairweather fault, southeast Alaska, and evidence for predecessors of the 1958 rupture: Geosphere, v. 17, p. 711–738, https://doi.org/10.1130/GES02299.1.
- Worthington, L.L., Van Avendonk, H.J., Gulick, S.P., Christeson, G.L., and Pavlis, T.L., 2012, Crustal structure of the Yakutat terrane and the evolution of subduction and collision in southern Alaska: Journal of Geophysical Research: Solid Earth, v. 117, B01102, https://doi.org/10.1029/2011JB008493.